STUDIES OF PROPELLANT SLOSHING UNDER LOW-GRAVITY CONDITIONS

by

Franklin T. Dodge

FINAL REPORT

Contract No. NAS8-20290

Control No. DCN 1-X-75-10122(1F)

SwRI Project 02-1846

Prepared for

National Aeronautics and Space Administration

George C. Marshall Space Flight Center

Marshall Space Flight Center, Alabama 35812

October 10, 1970

SOUTHWEST RESEARCH INSTITUTE

SAN ANTONIO HOUSTON

SOUTHWEST RESEARCH INSTITUTE
Post Office Drawer 28510, 8500 Culebra Road
San Antonio, Texas 78228

STUDIES OF PROPELLANT SLOSHING UNDER LOW-GRAVITY CONDITIONS

by
Franklin T. Dodge

FINAL REPORT
Contract No. NAS8-20290
Control No. DCN 1-X-75-10122(1F)
SwRI Project 02-1846

Prepared for
National Aeronautics and Space Administration
George C. Marshall Space Flight Center
Marshall Space Flight Center, Alabama 35812

October 10, 1970

Approved:

H. Norman Abramson, Director
Department of Mechanical Sciences

ACKNOWLEDGEMENT

The research summarized in this report was conducted for NASA-MSFC, under Contract NAS 8-20290, during the period January 4, 1966 to October 10, 1970. The Project Manager was Dr. Franklin T. Dodge. Dr. Wen-Hwa Chu and Mr. Luis R. Garza made substantial contributions to the research. The staff of the SwRI Computer Laboratory handled the computer programming, and Mr. Donald R. Tauch and Mr. Dennis C. Scheidt rendered technical aid in the experiments.

Special thanks are given to Mr. James E. Laurence and his staff at NASA-LeRC for making the NASA electromagnetic facility available to SwRI, and to Mr. Stephen Papell and Mr. Otto Faber of NASA-LeRC for giving us a generous amount of their magnetic-colloid liquid.

The entire program was made possible by the continuing efforts of the NASA-MSFC technical monitors: Mr. Robert S. Ryan, Mr. Frank Bugg, and Mr. Harry Buchanan.

TABLE OF CONTENTS

I. SUMMARY OF RESEARCH

Before 1966, the problems of fuel sloshing and its suppression during thrusting or for large axial acceleration conditions (high Bond numbers) were well understood, but corresponding knowledge of their behavior during periods of low accelerations (low Bond numbers) was rather meagre and specialized. Consequently, the chief objectives of our research were to study lateral sloshing of liquids in axisymmetric tanks under *low-gravity* conditions and to derive equivalent mechanical models of the sloshing for use in stability and control analyses. We studied only liquids and tank materials that have a "zero-degree contact angle," for which the liquid free surface is highly curved in a low-gravity environment, because it is this condition which is apparently encountered in space vehicle applications.

Although the chief objectives of this study concerned low-gravity behavior, a study of flexible baffles for slosh suppression in high Bond number conditions constituted a small effort at the start of the research program. The results of this study are now additionally significant due to the suggestion by NASA that such baffles may be employed in the Space Shuttle Vehicle.

Experimental data during the low-gravity sloshing phase of the program were obtained by *simulating* a low-gravity environment. A preliminary study of possible simulation techniques indicated that we could obtain reliable data on slosh natural frequency, slosh forces, and slosh damping by using *small models* to achieve low values of the Bond number for various tank shapes. We subsequently refined this technique to where it is now a precise and sensitive research tool. The data obtained by this method are generally limited to Bond numbers greater than about 10, which still covers the range of interest for large vehicles in coasting orbits. To obtain data for smaller Bond numbers and thus to approach more closely zero-gravity, we also conducted a series of exploratory tests using a *magnetic-colloid liquid* and a solenoidal magnet field such that the effective gravity acting on the liquid could be varied at will. Even though it was not possible to completely optimize our experimental method during the contract period, we obtained reliable data for effective gravities as small as 1 percent of standard gravity and Bond numbers as small as unity. We believe that with further refinement the magnetic liquid method could be made to yield reliable data at effective gravity levels of an order of magnitude smaller than we achieved in these preliminary tests.

The analytical work conducted for this contract dealt with the characteristics of inviscid fuel sloshing in axisymmetric tanks for arbitrary values of the Bond number, and we derived the first known equivalent mechanical model of fuel sloshing in low-gravity environments during the research. The culmination of the analytical efforts was a generalized computer program that predicts the natural frequencies and mode shapes for fuel sloshing in an arbitrary axisymmetric container.

The results of our program are detailed in ten technical reports and six published papers, which are discussed in the following section.

II. DOCUMENTATION

A. Technical Reports

Details of all aspects of the work performed on Contract NAS 8-20290 are given in the ten technical reports listed below. For convenience to the reader, the abstract of each report is given also.

1. Technical Report No. 1, "A Comparison of Flexible and Rigid Ring Baffles for Slosh Suppression," by Luis R. Garza, August 17, 1966.

   A test program to determine the effectiveness of flexible ring baffles as liquid slosh suppressors was conducted. A comparison of flexible and rigid ring baffles is presented in terms of liquid damping, first mode sloshing resonant frequency, and maximum baffle depth for no rotational slosh.

2. Technical Report No. 2, "Experimental and Theoretical Studies of Liquid Sloshing at Simulated Low Gravities," by Franklin T. Dodge and Luis R. Garza, October 20, 1966.

   An analysis is given for liquid sloshing in a rigid cylindrical tank under conditions of moderately low gravitational acceleration; the theory is valid for Bond numbers that are larger than 10. The results are put in the form of an equivalent mechanical model. It is found that both the fundamental sloshing mass and the natural frequency, for a liquid having a zero-degree contact angle, are smaller than for the usual high-g sloshing.

   A series of experiments was conducted to determine the sloshing force and the natural frequency for Bond numbers between 10 and 200. The test results are compared to the theoretical predictions of the mechanical model, and good correlation between theory and experiment is shown.

3. Technical Report No. 3, "A Discussion of Laboratory Methods of Simulating Low-Gravity Fluid Mechanics," by Franklin T. Dodge, February 1967.

   Methods of simulating the behavior of liquids in a low-gravity environment by experiments in Earth based laboratories are discussed, with an attempt made to point out the advantages and limitations of each. Two promising methods are indicated: small models, and magnetic liquids. It is concluded that these methods should be developed further, not only to complement orbital experiments but also to give preliminary data at low cost.

4. Technical Report No. 4, "Low Gravity Liquid Sloshing in an Arbitrary Axisymmetric Tank Performing Translational Oscillations," by Wen-Hwa Chu, March 20, 1967.

   The title problem is solved by using characteristic functions. The force and moment due to lateral translation of a rigid axisymmetric tank are obtained. However, no numerical example is given because of the considerable programming effort required.

5. Technical Report No. 5, "Simulated Low-Gravity Sloshing in Cylindrical Tanks Including Effects of Damping and Small Liquid Depth," by Franklin T. Dodge and Luis R. Garza, December 29, 1967.

   Liquid sloshing in cylindrical tanks is studied under conditions of simulated low gravities. The effects of finite liquid depths and the determination of the smooth wall damping are emphasized. The experimental and theoretical results show that the fluid dynamics are affected by small h/d ratios in much the same way as for normal, large Bond number sloshing. Measurements of the slosh damping indicate that the damping increases as the Bond number decreases, and two correlation equations for the damping factor are proposed. An equivalent mechanical model developed

previously is extended to include h/d variations and linear viscous damping. Comparisons of the force response predicted by the model to that measured in the tests verify the model to a high degree of confidence.

6. Technical Report No. 6, "Simulated Low-Gravity Sloshing in Spherical Tanks and Cylindrical Tanks with Inverted Ellipsoidal Bottoms," by Franklin T. Dodge and Luis R. Garza, February 1968 (includes errata sheet for Tech. Rept. No. 5).

   Liquid sloshing in cylindrical tanks having inverted ellipsoidal bottoms and in spherical tanks is studied experimentally under conditions of simulated low gravities. The effects of variable liquid depth and the determination of smooth wall damping are emphasized. Results from cylindrical tanks are qualitatively similar to results obtained previously with cylindrical tanks having flat bottoms; significant differences from previous results for natural frequency and slosh damping are apparent, however, for small liquid depths. Correlation equations for the damping coefficient as a function of h/d, N_{GA}, and N_{BO} are presented. Results from spherical tanks show that the variation in free-surface curvature with liquid depth has a strong effect on the natural frequency; in fact, increased curvature in spherical tanks as compared to cylindrical tanks causes the natural frequency to decrease as N_{BO} decreases, which is just the opposite of the variation obtained with cylindrical tanks. The damping in spherical tanks is shown to be a minimum when the tank is half-full; when $h_{av}/d = 0.50$ (half-full), γ_s is about 50% less than γ_s when $h_{av}/d = 0.25$, and about 10 to 20% less than when $h_{av}/d = 0.75$.

7. Technical Report No. 7, "Slosh Force, Natural Frequency, and Damping of Low-Gravity Sloshing in Oblate Ellipsoidal Tanks," by Franklin T. Dodge and Luis R. Garza, February 1969.

   Liquid sloshing in oblate ellipsoidal tanks is studied experimentally under conditions of simulated low gravities. The results demonstrate that the variation of free-surface curvature with liquid depth has a strong influence on natural frequency; for tanks over one-half full, the frequency decreases markedly as the Bond number is decreased. Moreover, the force response characteristics show that the mass of liquid participating in the sloshing is, in every case, less than the corresponding sloshing mass for a flat free surface. Calculations of the slosh damping show it to be a function of the liquid level, the Bond number, and the Galileo number.

8. Technical Report No. 8, "Low-Gravity Fuel Sloshing in an Arbitrary Axisymmetric Rigid Tank," by Wen-Hwa Chu, April 1969.

   Solutions to free and forced oscillations have been found in terms of an auxiliary set of eigenfunctions. The slosh force and moment for an arbitrary axisymmetric rigid tank at arbitrary Bond number have been derived for both pitching and translation and expressed in terms of characteristics of an equivalent spring-mass system. Numerical examples have been constructed which compare favorably with available theories and experiments.

9. Technical Report No. 9, "Magnetic Fluid Simulation of Liquid Sloshing in Low Gravity," by Franklin T. Dodge and Luis R. Garza, August 1970.

   An exploratory series of tests of simulated low-gravity liquid sloshing using a magnetic-colloid liquid in conjunction with a solenoidal magnetic field is described herein. A description of the experimental apparatus and test procedure is also presented.

   The magnetic body-force exerted on the liquid was varied by changing the magnetic field strength in order to obtain effective gravities as small as 0.01 g. The measured slosh natural frequencies for both cylindrical and spherical tanks in these low-gravity conditions agreed very well with theoretical predictions. Slosh damping, however, was significantly larger than expected because of the increase in viscosity of magnetic liquids due to magnetic field effects.

A magnetic-fluid analysis of sloshing is presented, and indicates that some deviation from true low-gravity behavior might occur whenever the Bond number is smaller than one. The discrepancy is caused by a magnetic interaction at the free surface that induces a jump in liquid pressure similar to that induced by surface tension.

10. Technical Report No. 10, "A Computer Program for Fuel Sloshing in an Axisymmetric Tank," by W. H. Chu, R. Gonzales, A. F. Muller, and D. R. Saathoff, August 1970.

    This report describes the use of the computer program developed to implement the analyses presented in Technical Report No. 8.

B. Published Papers and Notes

Five published technical papers and notes present the main results of the research program through Technical Report No. 8. A further paper is being prepared to present the results given in Technical Report No. 9.

Titles of the published material are listed below, and a reprint of each publication is given in the Appendix.

1. Garza, Luis R., and Dodge, Franklin T., "A Comparison of Flexible and Rigid Ring Baffles for Slosh Suppression," *AIAA Journal of Spacecraft and Rockets,* **4**, No. 6, June 1967, pp 805-806.

2. Dodge, F. T., and Garza, L. R., "Experimental and Theoretical Studies of Liquid Sloshing at Simulated Low Gravity," *Transactions ASME, Journal of Applied Mechanics,* **34**, No. 3, Sept. 1967, pp 555-561.

3. Dodge, Franklin T., and Garza, L. R., "Simulated Low-Gravity Sloshing in Cylindrical Tanks Including Effects of Damping and Small Liquid Depth," **Proceedings of the 1968 Heat Transfer and Fluid Mechanics Institute**, Ashley F. Emery and Creighton A. Depew, Editors, Stanford University Press, 1968, pp 67-79.

4. Dodge, Franklin T., and Garza, Luis R., "Simulated Low-Gravity Sloshing in Spherical, Ellipsoidal, and Cylindrical Tanks," *AIAA Journal of Spacecraft and Rockets,* **7**, No. 2, February 1970, pp 204-206.

5. Chu, Wen-Hwa, "A Theory for Low-Gravity Fuel Sloshing in an Arbitrary Axisymmetric Rigid Tank," ASME Paper No. 70-APM-EEE. To appear in *Transactions ASME, Journal of Applied Mechanics.*

6. Dodge, Franklin T., and Garza, Luis R., "Magnetic Fluid Simulation of Sloshing in Low Gravity," paper in preparation.

APPENDIX

Reprints of Papers and Notes Issued Under Contract NAS 8-20290

1. A Comparison of Flexible and Rigid Ring Baffles for Slosh Suppression
2. Experimental and Theoretical Studies of Liquid Sloshing at Simulated Low-Gravity
3. Simulated Low-Gravity Sloshing in Cylindrical Tanks Including Effects of Damping and Small Liquid Depth
4. Simulated Low-Gravity Sloshing in Spherical, Ellipsoidal, and Cylindrical Tanks
5. A Theory for Low-Gravity Fuel Sloshing in an Arbitrary Axisymmetric Rigid Tank

A Comparison of Flexible and Rigid Ring Baffles for Slosh Suppression

LUIS R. GARZA*
AND
FRANKLIN T. DODGE†
Southwest Research Institute, San Antonio, Texas

Introduction

THE stability of liquid-fuel-filled launch vehicles depends largely on the suppression of propellant sloshing. Many types of slosh suppression devices have been examined, and it has been found that ring baffles generally provide good damping characteristics.[1-4] To reduce the weight of the baffles, lightweight flexible baffles have been suggested. Stephens[5] presented data on the damping obtained from various flexible baffles in a rectangular tank and found that flexible baffles not only would be lighter but also would increase the liquid damping effectiveness. These interesting results led to the present studies of flexible ring baffles in a cylindrical tank.

Tank Configuration and Test Procedure

The experimental equipment and procedures utilized in the present work are similar to those employed in Ref. 6. Resultant liquid force on the tank wall, tank excitation amplitude, and liquid slosh height were recorded. The 17.75-in.-diam tank was made in two halves, each 17.75 in. long, with the baffles clamped between the flanges joining the tank halves. The damping and changes in natural frequencies were attributed only to the baffle, since in all these tests the bare wall tank (no baffle) damping was very small at the translational excitation amplitudes tested. The damping values in all cases were computed from the force-response curves by the half-bandwidth technique. For reference, a rigid baffle (made of $\frac{1}{8}$-in.-thick aluminum) was tested. The flexible baffles were made of Mylar plastic in four thicknesses: 0.002, 0.003, 0.005, and 0.0075 in. In every case, the ratio of the baffle width to tank radius was 0.157.

Results

Figure 1 shows damping ratio vs baffle depth for the rigid and the various flexible baffles for a single translation amplitude of $X_0/d = 0.00152$. The damping from the rigid baffle is slightly greater than that of the flexible baffles for baffle depths $0 < d_s/R \lesssim 0.025$, where d_s is the actual depth of the baffle below the undisturbed free surface, and R is the tank radius. However, for greater baffle depths the various flexible baffles are more effective; of these, the 0.002- and 0.003-in. Mylar baffles appear to be the most effective. Similar results are obtained for other excitation amplitudes. No rotational slosh was encountered in this particular series of tests; however, for larger excitation amplitudes, rotational slosh does occur for larger baffle submergence depths.

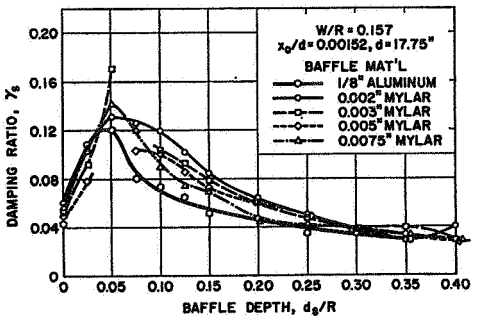

Fig. 1 Damping coefficients for rigid and various flexible baffles, excitation amplitude $X_0/d = 0.00152$.

If the liquid depth in the tank is at least as great as the tank diameter, the experimentally determined damping data for rigid ring baffles can be correlated with (i.e., are a function of) three dimensionless parameters: the ratio of the maximum wave height to the tank diameter (or alternatively, the excitation amplitude to the tank diameter); the ratio of the baffle submergence depth to the tank radius or diameter; and the ratio of the baffle width to the tank radius. These conclusions are also predicted by Miles' theory.[3] A dimensionless analysis for flexible baffles shows that one more parameter is needed here; the additional parameter is related to the flexibility of the baffle. For example, Stephens[5] correlated his data with the aid of a flexibility parameter defined as $F = (W/t)^3(1 - \mu^2)(\rho W^2/ET^2)$ where t = baffle thickness; W = baffle width; μ = Poisson's ratio; ρ = liquid density; E = modulus of elasticity; and T = period of slosh oscillation. He also used a period parameter P, but this parameter is equal to the already defined wave height-to-tank diameter parameter times the exponential function that accounts for the baffle depth.[3] In the present tests, a meaningful wave height could not be determined when the baffle was near the free surface (and for this reason the ratio of the excitation amplitude to tank diameter was used in place of the wave height parameter in most of our work), but in Fig. 2 curves are shown for the relative damping (flexible/rigid) parameter as functions of the period, flexibility, and baffle depth parameters for those cases in which the wave height could be measured. Each flexible baffle corresponds to one flexibility parameter in these plots; for example, the 0.003-in.-thick Mylar baffle corresponds to $F \approx 0.04$. The damping data for all of the baffles do correlate fairly well with these parameters.

Another flexibility parameter is the natural frequency Ω of the baffle in liquid (for the first antisymmetric ($\cos\theta$) mode) divided by the sloshing natural frequency. It was conjectured that the maximum damping would be provided by a baffle having a value of unity for this kind of flexibility parameter. To check this conclusion, the baffle natural frequency was computed by using hydrodynamic strip theory

Received December 16, 1966; revision received March 1, 1967. The results presented in this Note were obtained during research sponsored by NASA Marshall Space Flight Center under Contract NAS8-20290. More complete results are given in Technical Report 1, Contract NAS8-20290, Southwest Research Institute, August 1966. The authors thank Dr. Gordon L. Dugger for his considerable editing of the manuscript. [6.04, 7.09]

* Senior Research Engineer, Department of Mechanical Sciences.

† Senior Research Engineer, Department of Mechanical Sciences. Member AIAA.

Reprinted from JOURNAL OF SPACECRAFT AND ROCKETS

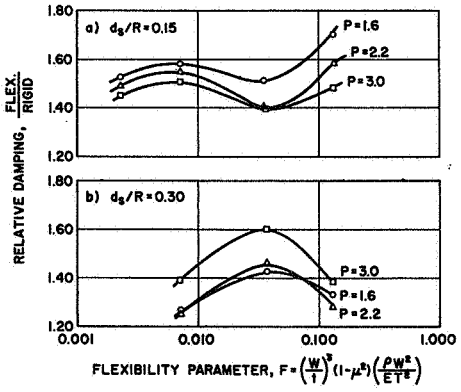

Fig. 2 Relative damping ratio vs flexibility parameter and period parameter: a) baffle submergence depth d_s/R = 0.15; b) baffle submergence depth d_s/R = 0.30.

and the elastic plate equation‡; the pertinent differential equation is

$$\frac{Et^3}{12(1-\mu^2)}\left[\frac{d^2}{dr^2}+\frac{1}{r}\frac{d}{dr}-\frac{1}{r^2}\right]^2 y - \Omega^2\left[t\rho_b + W\rho\left(1-\frac{r^2}{W^2}\right)^{1/2}\right] y = 0$$

where $y(r)\cos\theta$ is the assumed mode shape, ρ_b the baffle density and Ω the natural frequency of the baffle. This equation with appropriate boundary conditions was solved numerically, with the results shown in Fig. 3. According to this graph, the 0.003-in.-thick Mylar baffle has a natural frequency very close to the range of experimental slosh frequencies. From Fig. 2b, it can be seen that this baffle ($F \approx 0.04$) does indeed give the largest damping; however, this is true only for relatively large baffle submergence depths, as Fig. 2a shows that for shallower depths the more rigid baffles provide the highest damping. This last fact is even more clearly illustrated in Fig. 1.

Conclusions

In general, test results indicate that lightweight, flexible ring baffles provide damping about equal to or even better than similar rigid baffles. For baffles not too close to the free surface, the relative damping varies from an approximate value of 2 for small excitation amplitudes to a value slightly greater than 1 for larger amplitudes. The more flexible baffles provided the higher damping values (except when placed near the free surface) and also maintained a more constant liquid resonant frequency throughout the baffle depth range investigated. It appears to be logical to select a baffle whose natural frequency equals the sloshing natural frequency; such a baffle gives the best damping for deeply submerged baffles and gives fairly good damping characteristics for shallower submergence.

There is no question but that flexible baffles can reduce baffle weight by a considerable amount; however, the properties of the baffle material at cryogenic temperatures must be evaluated, and it may be necessary to investigate the stresses at the baffle inner edge to insure that tearing will not occur.

‡ This analysis was formulated by W.-H. Chu of Southwest Research Institute, to whom the authors express their appreciation.

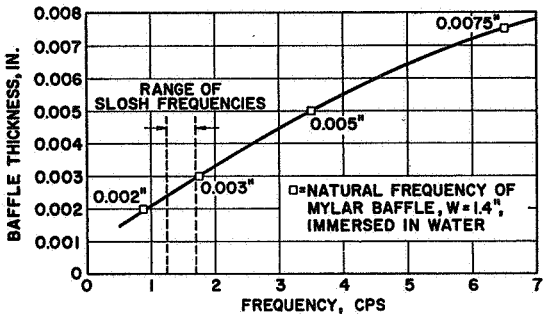

Fig. 3 Natural frequency of flexible baffle as a function of thickness.

References

[1] Silveira, M. A., Stephens, D. G., and Leonard, H. W., "An experimental investigation of the damping of liquid oscillations in cylindrical tanks with various baffles," NASA TN D-715 (May 1961).

[2] Miles, J. W., "Ring damping of free surface oscillations in a circular tank," J. Appl. Mech. **25**, 274–276 (June 1958).

[3] Abramson, H. N. and Garza, L. R., "Some measurements of the effects of ring baffles in cylindrical tanks," J. Spacecraft Rockets **1**, 560–562 (1964).

[4] Garza, L. R., "Theoretical and experimental pressures and forces on a ring baffle under sloshing conditions," J. Spacecraft Rockets **3**, 276–278 (1966).

[5] Stephens, D. G., "Flexible baffles for slosh damping," J. Spacecraft Rockets **3**, 765–766 (1966).

[6] Abramson, H. N. and Ransleben, G. E., Jr., "Simulation of fuel sloshing characteristics in missile tanks by use of small models," ARS J. **30**, 603–612 (July 1960).

F. T. DODGE
Senior Research Engineer.
Assoc. Mem. ASME

L. R. GARZA
Research Engineer.

Department of Mechanical Sciences,
Southwest Research Institute,
San Antonio, Texas

Experimental and Theoretical Studies of Liquid Sloshing at Simulated Low Gravity[1]

Analyses and experimental comparisons are given for liquid sloshing in a rigid cylindrical tank under conditions of moderately small axial accelerations; in particular, the theory is valid for Bond numbers larger than 10. The analytical results are put in the form of an equivalent mechanical model, and it is shown that the sloshing mass and the natural frequency of the first mode, for a liquid having a 0 deg contact angle at the tank walls, are smaller than for high-g conditions. The experimental data, obtained by using several small-diameter tanks and three different liquids, are compared to the predictions of the mechanical model; good correlation is found in most cases for the sloshing forces and natural frequency as a function of Bond number.

Introduction

THE FREE surface wave motion, or sloshing, of liquid fuel in large rocket boosters is a well-recognized problem in technology. Results are available for lateral sloshing [1, 2],[2] nonlinear aspects [3], vertical sloshing, i.e., sloshing in which the excitation of the tank is in the axial direction [4, 5], and other phenomena [6]. Nearly all the experimental and theoretical work has been limited, however, to situations in which the steady axial acceleration of the tank (gravity or thrust or both) is large; thus the liquid's motion can be determined by considering only the body forces in the liquid and the forces arising at the walls of the tank. But there are occasions when the axial acceleration is small, as for example, when the booster is coasting in an earth orbit, and then other forces must be taken into account; the most important of these forces is usually the interfacial tension between the liquid fuel and the ullage gas. The resulting free surface motion under such conditions is called "low-gravity" sloshing.

Most of the previous research on low-gravity fluid mechanics is reviewed in [7], which also contains a lengthy reference list. The reports by Reynolds and his co-workers [8, 9] are especially recommended. Some recent work is given in [10, 11]. However, to the authors' knowledge, there are no experimental or explicit theoretical results available for the important problem of sloshing during forced excitation of the tank (although the generalized analysis of [10] supposedly can be specialized to include this). In particular, there is a complete lack of experimental data for the dynamic forces exerted by the sloshing liquid. Thus, in this paper, analytical and experimental results for low-gravity sloshing in a rigid cylindrical tank are presented for the case of simple harmonic translation of the tank.

Experimental data for low-gravity sloshing are not obtained easily. Laboratory facilities that can duplicate an actual small axial acceleration, such as drop towers, are usually not able to provide the low-gravity field for a sufficiently long duration to get consistent and reliable sloshing data. An alternative method of *simulating* low gravity is to use models of small dimensions; in this way, the interfacial or capillary forces can be made comparable to, or greater than, the gravity or body forces even in the standard gravity field; thus this is a suitable "low-gravity" test for some purposes. The available test time is not a problem with this kind of simulation, but the liquid motion and the slosh forces are very small because of the smallness of the model tank. In the experiments reported here, the simulation was accomplished through this use of small models; such a simulation required that an extremely sensitive and precise dynamometer system be constructed since slosh forces on the order of 0.0001 lb were expected. As far as is known to the authors, the data presented here are the first, and the only up to now, that give sloshing forces and frequencies for low gravitational (i.e., small Bond number) conditions. (However, some data for natural frequencies have been published previously [9].)

The Bond numbers ($N_{BO} = \rho g R_0^2/T$ is an indication of the size of body forces relative to interfacial forces[3]) used in the tests were in the range of 10 to 100. Now, very low-gravity fluid mechanics are characterized by $N_{BO} < 1$ while high-g problems occur for

[1] The results presented in this paper were obtained during the course of research sponsored by the NASA Marshall Space Flight Center under Contract NAS8-20290.

[2] Numbers in brackets designate References at end of paper.

Contributed by the Applied Mechanics Division and presented at the Applied Mechanics Conference, Pasadena, Calif., June 26–28, 1967, of THE AMERICAN SOCIETY OF MECHANICAL ENGINEERS.

Discussion of this paper should be addressed to the Editorial Department, ASME, United Engineering Center, 345 East 47th Street, New York, N. Y. 10017, and will be accepted until October 15, 1967. Discussion received after the closing date will be returned. Manuscript received by ASME Applied Mechanics Division, November 14, 1966. Paper No. 67—APM-14.

[3] See Nomenclature for definition of symbols.

Nomenclature

NOTE: Symbols in parentheses are the nondimensional equivalents of the preceding quantity.

a_n = expansion coefficient in series for Φ; see equation (9)
b_n = expansion coefficient in series for ϵ; see equation (10)
$C1_{nm}$, $C2_{nm}$, $C3_{nm}$ = Fourier-Bessel coefficients in equations (11) and (12)
$f(F)$ = height of meniscus above $Z = 0$; see Fig. 1
F_L = lateral force exerted on tank by liquid
g = steady axial acceleration or gravity
$J_1(\lambda_n R)$ = first-order Bessel function of first kind
M = number of terms in series for Φ and ϵ, or number of slosh masses
N_{BO} = Bond number, $\rho g R_0^2/T$
$r(R)$, θ, $z(Z)$ = axes of tank-fixed coordinate system; see Fig. 1
$t(\tau)$ = time
T = interfacial tension
$x_0(X_0)$ = excitation amplitude
β = nondimensional meniscus height at tank wall
ζ = total wave height above $Z = 0$; see Fig. 1
$\eta(\epsilon)$ = wave height above meniscus; see Fig. 1
λ_n = roots of $J_1'(\lambda_n) = 0$
ρ = density of liquid
$\phi(\Phi)$ = velocity potential
Ω_n = dimensionless natural frequency of nth mode
$\omega(\Omega)$ = excitation frequency

$N_{BO} > 1000$. Thus $10 < N_{BO} < 100$ should be classified as moderately low-gravity problems; Bond numbers of this size, for example, are encountered in coasting orbits of some large rocket boosters where the effective axial acceleration is only about 2×10^{-5} of standard gravity [12]. Even though body forces are still dominant, but not overwhelmingly so, for $10 < N_{BO} < 100$, interfacial tension causes the undisturbed free surface to depart considerably from the usual flat surface and, hence, interfacial curvature and forces must be included in the analysis.

Analysis

Effects such as stratification or thermally driven motions are ignored in the analysis and are absent in the experiments. The influence of viscosity is also neglected in the analysis since experience has shown it to be small and accountable for a posteriori by adding suitable linear damping. In other words, the usual sloshing assumptions are made: Incompressible, ideal liquid; irrotational motions; negligible inertia of the ullage gas. An r, θ, z cylindrical coordinate system is *fixed* to the tank and centered along the axis at the point it intersects the undisturbed free surface, as shown in Fig. 1. The depth of liquid below $z = 0$ is taken to be so large that the tank bottom is essentially at $z = -\infty$; this greatly simplifies the algebraic labor and is valid if $h/2R_0 > 1$. The height, $f(r)$, of the undisturbed, axisymmetric free surface is measured positively above $z = 0$, and the wave height $\eta(r, \theta, t)$ is then measured from this surface and not from $z = 0$.

A velocity potential $\phi(r, \theta, z, t)$ is defined such that the liquid's velocity relative to the tank is $\mathbf{V} = \nabla\phi$. The equations are immediately made nondimensional by dividing all quantities having the dimensions of length by R_0 and those having the dimensions of time by $(R_0/g)^{1/2}$; for example, the nondimensional wave height is $\epsilon(R, \theta, \tau) = \eta(r/R_0, \theta, t\sqrt{g/R_0})/R_0$ and the nondimensional frequency is $\Omega = \omega(R_0/g)^{1/2}$.[4] Furthermore, the nonlinear boundary conditions at the free surface are linearized by assuming that Φ and ϵ are small compared to unity; note that this does *not* imply that the equilibrium shape $f(r)$ need be nearly plane. The complete set of nonlinear equations could probably be solved by methods similar to those outlined in [3], or by Hutton [13], or by Dodge, et al. [5], but a nonlinear analysis is not usually warranted in applications and, in addition, a linear analysis serves to point out the main differences between low-gravity sloshing and the usual high-g sloshing.

[4] For very small Bond numbers, a better nondimensionalization of time is obtained by using $(\rho R_0^3/T)^{1/2}$ as the significant time. This avoids any difficulties that might arise as $g \to 0$.

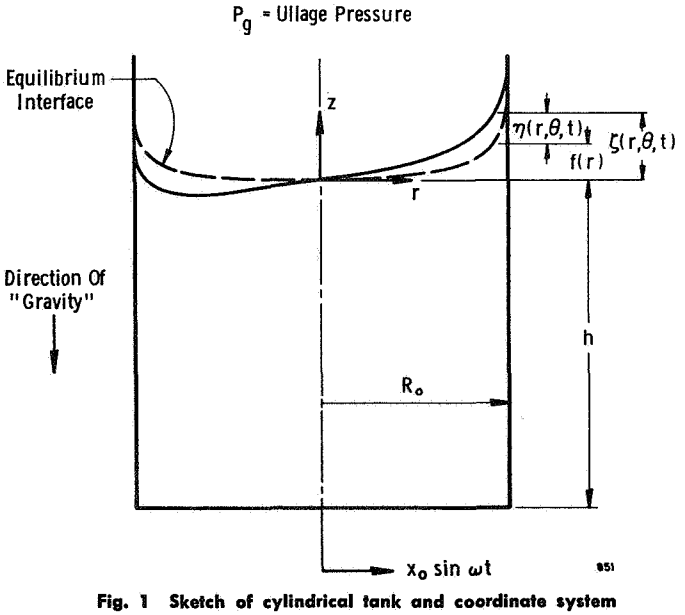

Fig. 1 Sketch of cylindrical tank and coordinate system

The potential must satisfy Laplace's equation

$$\nabla^2\Phi = 0 \text{ in the liquid} \tag{1}$$

and two conditions at the tank boundaries

$$\partial\Phi/\partial R = 0, \qquad R = 1 \tag{2}$$

$$\partial\Phi/\partial Z = 0, \qquad Z = -\infty \tag{3}$$

The first integral of the equations of motion evaluated just below the free surface gives one relation between the velocity potential and the wave height; another condition is obtained by requiring that the normal pressure across the free surface must be discontinuous by an amount proportional to the product of the interfacial tension and the mean surface curvature. By combining these two equations and linearizing with respect to Φ and ϵ, as shown in [16], one relation results:

$$\frac{\partial\Phi}{\partial\tau} + \epsilon - \frac{1}{N_{BO}}\left(\frac{1}{R}\frac{\partial}{\partial R}\left\{\frac{R\dfrac{\partial\epsilon}{\partial R}}{\left[1+\left(\dfrac{dF}{dR}\right)^2\right]^{3/2}}\right\} + \frac{1}{R^2}\frac{\partial}{\partial\theta}\left\{\frac{\dfrac{\partial\epsilon}{\partial\theta}}{\left[1+\left(\dfrac{dF}{dR}\right)^2\right]^{1/2}}\right\}\right) - X_0\Omega^2 R\cos\theta\sin\Omega\tau = 0, \qquad Z = F \tag{4}$$

A second condition between the potential and the wave height arises from the fact that the motion of the free surface and the fluid velocity at the surface must be consistent with each other; linearized, this condition is

$$\frac{\partial\epsilon}{\partial\tau} - \frac{\partial\Phi}{\partial Z} + \frac{dF}{dR}\left(\frac{\partial\Phi}{\partial R}\right) = 0, \qquad Z = F \tag{5}$$

The final requirement for a well-posed problem is knowledge of the angle at which the free surface meets the tank walls.[5] It is assumed here that the contact angle measured in the liquid, for the undisturbed surface, is zero, which is typical of several existing fuel-tank systems. However, it is entirely possible that the angle at which the moving wave meets the wall is not the same as the static contact angle; this phenomenon is known as contact angle hysteresis. Some researchers have tried to account for the hysteresis by assuming that

$$\partial\epsilon/\partial R = C_1\epsilon, \qquad R = 1 \qquad Z = F(1)$$

which seems to imply that the change in the contact angle depends only on the distance the free surface is displaced from equilibrium. If C_1 is truly a constant, this equation does not seem able to explain the damping or energy dissipation caused by the hysteresis. The entire subject of contact angle hysteresis and surface wave damping has recently been reviewed by Miles [14], and he points out that the important physical processes are far from being fully understood. Thus, rather than postulate an arbitrary functional relationship, hysteresis is neglected in the analysis, and the contact line is assumed to slide easily along the tank walls—the so-called "free edge" condition. In other words, the contact angle condition used here is

$$\partial\epsilon/\partial R = 0, \qquad R = 1 \qquad Z = F(1) \tag{6}$$

Since the contact angle is defined by

$$\theta_c = \cot^{-1}\left\{\frac{\partial\zeta}{\partial r}\Big/\left[1+\left(\frac{\partial\zeta}{r\partial\theta}\right)^2\right]^{1/2}\right\}$$

(at $r = R_0$), equation (6) actually implies that θ_c is always equal

[5] In high-g analyses, the free surface is flat at equilibrium and is assumed to deform to whatever shape the dynamics require, regardless of the value of the contact angle.

to zero in the linearized approximations used here.[6]

It is clear that the equilibrium free surface shape, $F(R)$, must be known before an analysis of the sloshing can be completed. Exact computations of $F(R)$ can be quite involved [10] but, fortunately, very good approximate expressions can be derived for the range of Bond numbers of interest here. For $N_{BO} \ll 1$, the equilibrium interface is nearly spherical; that is, $F(R) = 1 - (1 - R^2)^{1/2}$. As N_{BO} increases, the interface becomes flatter. Using this as a guide, Satterlee and Chin [15] showed that a modified spherical shape, $F(R) = \beta[1 - (1 - R^2)^{1/2}]$ with β a function of N_{BO}, was an approximate solution of the equations that agreed well with experiments and exact solutions for $N_{BO} < 10$. For large N_{BO}, the assumed shape, however, was not "flat" enough. Thus, for $10 < N_{BO} < 100$, a reasonable assumption is

$$F(R) = \beta[1 - (1 - R^2)^{1/2}] \tag{7}$$

since the curvature of this is considerably less than that of the modified spherical shape. Equation (7) already satisfies the boundary conditions that $F(0) = dF(0)/dR = 0$ and $dF(1)/dR = \cot \theta_c = \infty$; by substituting it into the equilibrium analog of equation (4), it can be seen that equation (7) also satisfies the correct interface curvature-pressure relation at $R = 0$. Thus reasonable predictions of β, the nondimensional height of the meniscus at the tank wall, can be obtained by forcing equation (7) to satisfy this relation at $R = 1$. Doing this gives the result:

$$\beta^2 N_{BO} - \beta^2 - (2/3) = 0 \tag{8}$$

Equations (7) and (8) agree fairly well with the experimental data of [15] for $N_{BO} > 10$.

Even after linearizing the equations and assuming a relatively simple expression for $F(R)$, the authors know of no function or set of functions that will exactly satisfy all of equations (1–6). Of several approximate methods, the one selected here is to construct a solution from the known set of functions for sloshing when $N_{BO} = \infty$, i.e., $F = 0$. This seems logical because body forces are still the largest forces when $N_{BO} > 10$. Thus it is assumed that the velocity potential is

$$\Phi(R, \theta, Z, \tau) = \sum_{n=1}^{\infty} a_n(\tau) \cdot J_1(\lambda_n R) \cdot \cos \theta \cdot e^{\lambda_n Z} \tag{9}$$

and the wave shape is

$$\epsilon(R, \theta, \tau) = \sum_{n=1}^{\infty} b_n(\tau) \cdot J_1(\lambda_n R) \cdot \cos \theta \tag{10}$$

These two series expansions will identically satisfy equations (1), (2), (3), and (6) if λ_n are the roots of $J_1'(\lambda_n) = 0$. This will also insure that each $J_1(\lambda_n R)$ is orthogonal to all the rest in the interval $0 \leq R \leq 1$, with the weighting function equal to R. (Note, however, that the expansion for ϵ cannot be made to satisfy a contact line condition of the form $\partial\epsilon/\partial R = C_1\epsilon$ if $C_1 \neq 0$.)

Now equations (9) and (10) are substituted into the boundary conditions, equations (4) and (5), in order to determine the a_n and b_n. The resulting two equations are then expanded again into a Bessel-Fourier series of $J_1(\lambda_m R) \cos \theta$ terms. The results for equation (5) are

$$\sum_{n=1}^{\infty} \left\{ \dot{b}_n + \sum_{m=1}^{\infty} C1_{nm} a_m \right\} J_1(\lambda_n R) \cos \theta = 0 \tag{11}$$

and for equation (4)

$$\sum_{n=1}^{\infty} \left\{ b_n + \sum_{m=1}^{\infty} C2_{nm} \dot{a}_m + \sum_{m=1}^{\infty} C3_{nm} b_m - \frac{2X_0\Omega^2}{(\lambda_n^2 - 1)J_1(\lambda_n)} \sin \Omega\tau \right\} J_1(\lambda_n R) \cos \theta = 0 \tag{12}$$

where the superscript dots indicate time differentiation, and $C1_{nm}$, $C2_{nm}$, and $C3_{nm}$ are the functions of β and N_{BO} given in the Appendix. After combining these two equations to eliminate the $b_n(\tau)$ and noting that each term in the sum over n must be identically zero, the resulting equations for the $a_n(\tau)$ are

$$\sum_{m=1}^{\infty} C2_{nm} \ddot{a}_m - \sum_{m=1}^{\infty} C1_{nm} a_m - \sum_{s=1}^{\infty} \left(C3_{ns} \sum_{m=1}^{\infty} C1_{sm} a_m \right) = \frac{2X_0\Omega^2}{(\lambda_n^2 - 1)J_1(\lambda_n)} \cos \Omega\tau = 0 \qquad n = 1, 2, 3, \ldots \tag{13}$$

It follows that each a_n depends on all the rest. Adequate results, nonetheless, can be obtained for the first few modes by truncating the equations at, say, $n = m = M$ and then solving the set of equations by ordinary methods.

Only the steady-state response is desired, so, by letting $a_n = A_n \cos \Omega\tau$ and substituting this into equation (13) (after truncating at $n = m = M$), the A_n can be calculated:

$$A_n = \left[\frac{K_{1n}\Omega^{2M} + K_{2n}\Omega^{2M-2} + \ldots + K_{Mn}\Omega^2}{\Omega^{2M} + K_1\Omega^{2M-2} + \ldots + K_{M-1}\Omega^2 + K_M} \right] X_0\Omega, \qquad n = 1, 2, \ldots, M \tag{14}$$

K_{ij} and K_i are various products of the constants in equations (13). Equation (14) can be put into a more revealing form by rearranging it according to the ideas of partial fractions:

$$A_n = \left[\frac{P_{1n}}{\Omega^2 - \Omega_1^2} + \frac{P_{2n}}{\Omega^2 - \Omega_2^2} + \ldots + \frac{P_{Mn}}{\Omega^2 - \Omega_M^2} \right] X_0\Omega^3, \qquad n = 1, 2, \ldots, M \tag{15}$$

The Ω_i^2, which are the factors of the denominator in equation (14), can be identified as the square of the natural frequency of the ith sloshing mode. They are ordered such that $\Omega_1^2 < \Omega_2^2 < \ldots < \Omega_M^2$. Physical reasoning implies that all the $\Omega_i^2 > 0$, and this turns out always to be the case.

By substituting these results in equation (9) and rearranging the terms according to natural frequency, the velocity potential works out to be

$$\Phi = X_0\Omega^3 \cos \theta \cos \Omega\tau \sum_{n=1}^{M} \frac{1}{\Omega^2 - \Omega_n^2} \times \left\{ \sum_{m=1}^{M} P_{nm} J_1(\lambda_m R) e^{\lambda_m Z} \right\} \tag{16}$$

The sum in braces in this equation is the normal mode function of the nth sloshing mode. Note that the index n in P_{nm} in equation (16) occupies the first position in the subscript while, in equation (15), it occupies the second; thus all the A_n contribute to each mode of Φ.

Similarly, by letting $b_n = B_n \sin \Omega\tau$, the wave shape is found to be

$$\epsilon = X_0\Omega^2 \cos \theta \sin \Omega\tau \sum_{n=1}^{M} \frac{1}{\Omega^2 - \Omega_n^2} \left\{ \sum_{m=1}^{M} Q_{nm} J_1(\lambda_m R) \right\} \tag{17}$$

where the Q_{ij} are various products of the P_{ij} and the constants in equation (11).[7]

The velocity potential and the wave shape have now been determined. Any particular sloshing mode can be studied by picking out the appropriate terms in equations (16) and (17); as will be seen, this is of considerable value in formulating an equivalent mechanical model. It should be emphasized that, once $C1_{nm}$, $C2_{nm}$, and $C3_{nm}$ are obtained by numerical integration with a computer, the remaining computations can be done by hand or with a desk calculator (at least as long as $M \leq 4$, which appears to be sufficient to give adequate results for the first

[6] $\zeta = f + \eta$, and so $(\partial\zeta/r\partial\theta)^2 = (\partial\eta/r\partial\theta)^2$, which may be neglected in comparison to unity. Also $\partial\zeta/\partial r = df/dr + \partial\eta/\partial r = df/dr$ at $r = R_0$, according to equation (6). Therefore, $\theta_c = \cot^{-1}(df/dr) = 0$ always.

[7] More complete details of the analysis and some numerical examples are given in [16]; they are omitted here for the sake of brevity.

mode). This is possibly an advantage not available with some other computation schemes.

Equivalent Mechanical Model

The sloshing characteristics important in missile applications (natural frequencies and forces and moments exerted on the tank) are displayed in a convenient form by an equivalent (mathematical) mechanical model. The proposed model for low-g sloshing is shown in Fig. 2; it is outwardly similar to models for high-g sloshing [1]. One spring-mass oscillator is included for each of the M slosh modes. The parameters of the model (m_0, m_n, h_0, h_n, k_n) are computed by matching the actual sloshing forces and moments with the forces and moments caused by the model for the same excitation.

The interfacial tension force acting on the tank walls along an element ds of the contact line is shown in Fig. 3; this force arises as a consequence of considering the interfacial tension to act similarly to a stretched membrane. $F_T = TR_0 d\theta$ is the linearized force in the plane of the wall (for a 0 deg contact angle) and the part of it acting in the increasing θ-direction is $F_{T,\theta} = F_T(\partial\eta/\partial\theta)$. The net force on the tank due directly to interfacial tension is a vertical force, not important here, and the vector sum of the $F_{T,\theta} \cdot ds$ forces, which turns out only to have a resultant in the direction of the tank excitation. Thus

$$F_1 = \int_0^{2\pi} -\frac{\partial\eta(r = R_0)}{\partial\theta} T \sin\theta d\theta = \left(\frac{1}{N_{BO}}\right) \times \pi\rho R_0^3 x_0\omega^2 \sin\omega t \sum_{n=1}^{M} \frac{H_n \frac{g}{R_0}}{\omega^2 - \Omega_n^2 \frac{g}{R_0}} \quad (18)$$

where $H_n = \sum_{m=1}^{M} Q_{nm} J_1(\lambda_m)$ is the dimensionless wave height at the wall for the nth mode.

The part of the force on the tank attributable directly to the liquid's motion can be calculated with the aid of Φ if a velocity potential for particles moving with the tank, $\Phi' = X_0\Omega R \cos\theta \times \cos\Omega\tau$, is added to it in order to make it valid in an inertia reference frame. Thus this part of the force is

$$F_2 = \rho g R_0^3 \int_0^{2\pi} \int_{-\frac{h}{R_0}}^{\beta+\epsilon_0} -\left[\frac{\partial\Phi(R = 1)}{\partial\tau} - X_0\Omega^2 \cos\theta \sin\Omega\tau + Z\right] \cos\theta dZ d\theta \quad (19)$$

where $\epsilon_0 = \epsilon(R = 1, \theta, \tau)$. The last term in the integral, the part equal to Z, is negligible for very large Bond numbers and, in such cases, the upper limit on the Z-integration is zero;[3] in this case, though, it has a nonnegligible part after linearization:

$$\int_0^{2\pi} \int_{-\frac{h}{R_0}}^{\beta+\epsilon_0} Z \cos\theta dZ d\theta = \beta \int_0^{2\pi} \epsilon_0 \cos\theta d\theta = \pi\beta X_0\Omega^2 \sin\Omega\tau \sum_{m=1}^{M} \frac{H_n}{\Omega^2 - \Omega_n^2} \quad (20)$$

Hence the force F_2 works out to be

$$F_2 = \pi\rho R_0^3 x_0\omega^2 \sin\omega t \left\{\beta + \frac{h}{R_0} - \beta \sum_{n=1}^{M} \frac{H_n \frac{g}{R_0}}{\omega^2 - \Omega_n^2 \frac{g}{R_0}} + \omega^2 \sum_{n=1}^{M} \frac{I_n}{\omega^2 - \Omega_n^2 \frac{g}{R_0}}\right\} \quad (21)$$

[3] That is, retaining the upper limit equal to ϵ_0 results only in higher-order terms in ϵ_0, which must eventually be discarded.

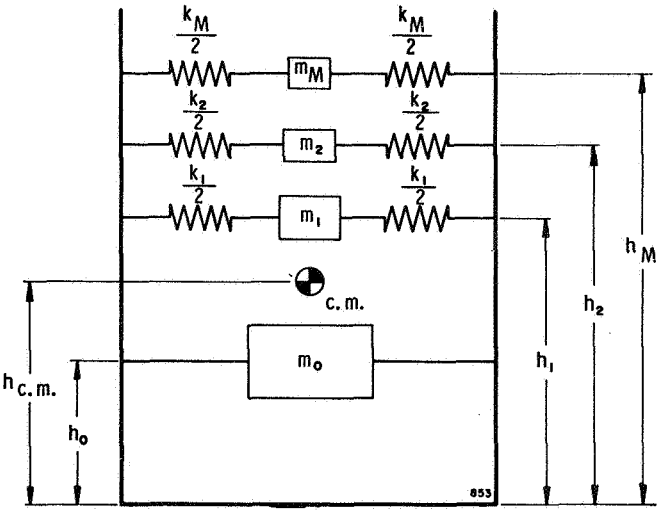

Fig. 2 Schematic of equivalent mechanical model

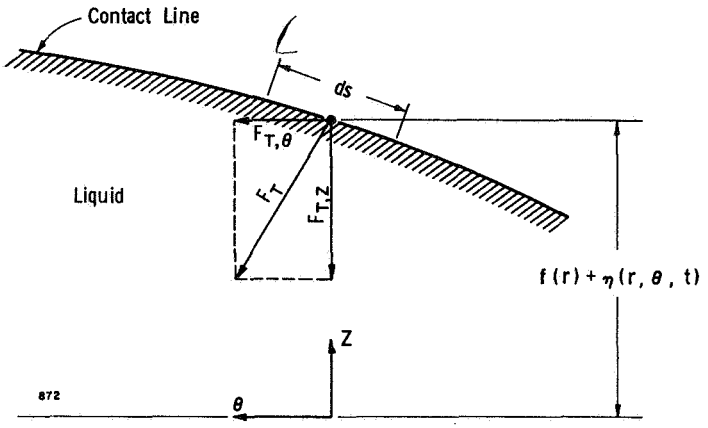

Fig. 3 Interfacial tension force at liquid-tank contact line

where $I_n = \sum_{m=1}^{M} \frac{P_{nm}}{\lambda_m} J_1(\lambda_m) e^{\lambda_m\beta}$. Now, combining F_1 and F_2 and rearranging various terms, the total lateral force on the tank is

$$F_L = \pi\rho R_0^3 x_0\omega^2 \sin\omega t \left\{\frac{h}{R_0} + \left[\beta + \left(\beta - \frac{1}{N_{BO}}\right) \sum_{n=1}^{M} \frac{H_n}{\Omega_n^2}\right] + \omega^2 \sum_{n=1}^{M} \frac{I_n - \left(\beta - \frac{1}{N_{BO}}\right) \frac{H_n}{\Omega_n^2}}{\omega^2 - \Omega_n^2 \frac{g}{R_0}}\right\} \quad (22)$$

By calculating the lateral force on the tank walls exerted by the system of masses and springs in the mechanical model, one finds

$$F_{\text{model}} = x_0\omega^2 \sin\omega t \left[m_0 + \sum_{n=1}^{M} m_n - \omega^2 \sum_{n=1}^{M} \frac{m_n}{\omega^2 - \frac{k_n}{m_n}}\right] \quad (23)$$

Comparing equations (22) and (23) shows that the mechanical model will give forces equivalent to the sloshing if

$$m_n = -\left[I_n - \left(\beta - \frac{1}{N_{BO}}\right) \frac{H_n}{\Omega_n^2}\right] \quad (24)$$

$$k_n/m_n = \Omega_n^2 (g/R_0) \quad (25)$$

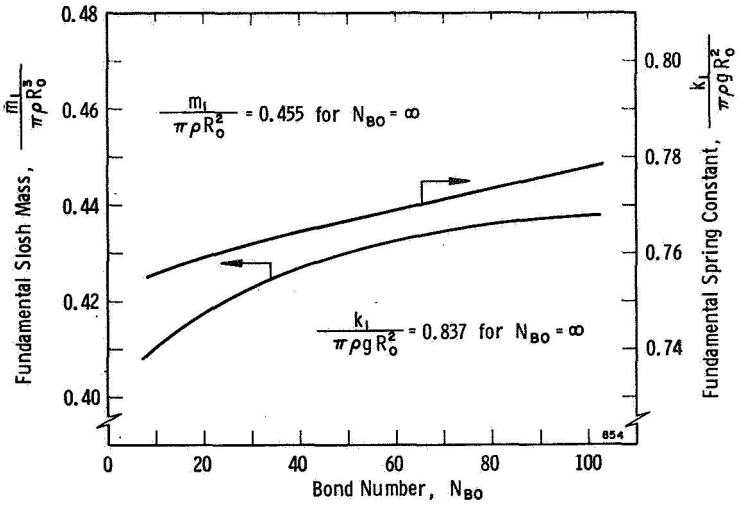

Fig. 4 Fundamental slosh mass and spring constant

and

$$m_0 + \sum_{n=1}^{M} m_n = \pi\rho R_0^3 \left[\frac{h}{R_0} + \beta + \left(\beta - \frac{1}{N_{BO}}\right) \sum_{n=1}^{M} \frac{H_n}{\Omega_n^2}\right] \tag{26}$$

Numerical calculations show that $\pi\rho R_0^3\left[\frac{h}{R_0} + \beta + \left(\beta - \frac{1}{N_{BO}}\right) \times \sum_{n=1}^{M} \frac{H_n}{\Omega_n^2}\right]$ is always very nearly equal to the total mass of the liquid, which is $m_T = \rho\pi R_0^3(h/R_0 + 0.264\beta)$; as $M \to \infty$, it is reasonable to assume that it would equal the liquid mass exactly (it would be surprising if it didn't), although this would probably be difficult to prove in complete generality. Assuming, then, that the term *is* equal to m_T, equation (26) shows that

$$m_0 + \sum_{n=1}^{M} m_n = m_T = \rho\pi R_0^3(h/R_0 + 0.264\beta) \tag{26'}$$

According to these equations, m_n and k_n can be computed from knowledge of only the nth sloshing mode and surface wave; i.e., the modes are not coupled. In Fig. 4, the fundamental sloshing mass m_1 and the fundamental spring constant k_1 are shown as functions of the Bond number. In every case, the amount of liquid participating in the sloshing motion is smaller than for $N_{BO} = \infty$; and, in fact, for $N_{BO} = 10$, the sloshing mass is almost 10 percent less than the high-g case. The amount of liquid participating in the second and higher modes is very small.

Carrying out the same kind of comparisons between the sloshing moment on the tank and the model moment results in the same values for m_0, m_n, and k_n; and, in addition, it is required that

$$h_n = R_0\left\{\frac{h}{R_0} - \frac{1}{\Omega_n^2} - \frac{\pi\rho R_0^3}{m_n}\left[\sum_{m=1}^{M}\left(\beta - \frac{1}{\lambda_m}\right) \times \frac{P_{nm}J_1(\lambda_m)e^{\lambda_m\beta}}{\lambda_m} - \beta\left(\beta - \frac{1}{N_{BO}}\right)\frac{H_n}{\Omega_n^2}\right]\right\} \tag{27}$$

and

$$h_0 = \frac{1}{m_0}\left(m_T h_{c.m.} - \sum_{n=1}^{M} m_n h_n\right) \tag{28}$$

where the center-of-mass coordinate above the tank bottom is

$$h_{c.m.} = R_0\left[\frac{\frac{h}{R_0} + 0.528\beta + 0.128\beta^2\frac{R_0}{h}}{2\left(1 + 0.264\beta\frac{R_0}{h}\right)}\right] \tag{29}$$

Again, h_n depends only on the nth sloshing mode. Also, for $N_{BO} = \infty$, in which case $\Omega_n^2 = \lambda_n$ and $P_{nm} = 0$ for $n \neq m$, equation (27) reduces to $h_n = h - (2R_0/\lambda_n)$, which is the correct result [1]. In every case, the line of action of the spring-mass is slightly nearer the bottom of the tank than for $N_{BO} = \infty$. Since the interest here is primarily in the forces, the results for h_0 and h_n are not presented graphically.

Experimental Results and Comparison With Theory

The main objective of the experimental program was to determine the sloshing force (for incompressible liquids in rigid cylindrical tanks) as a function of the excitation frequency for a frequency band centered about the fundamental mode, with the Bond number being the chief parameter. The apparatus used to accomplish this is shown in Fig. 5; the entire dynamometer-tank-base system is attached directly to the armature of an electrodynamic shaker, which provides the required translational excitation. As can be seen, there are two test tanks (the ones shown are approximately 1 in. dia). One tank, called the active tank, contains the test liquid, and the other tank, called the balance tank, is used to cancel the inertial signal of the empty active tank by appropriate electrical connections of the semiconductor strain gage dynamometer arms and the adding of balance weights; thus the signal recorded is that due only to the inertia of the sloshing liquid.

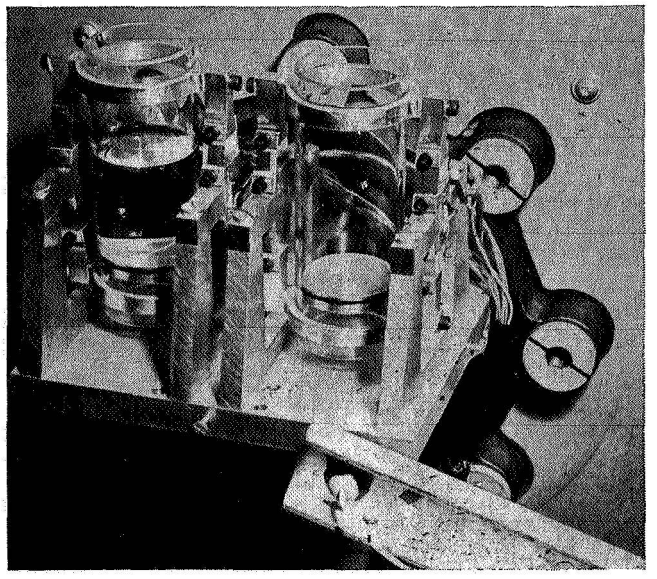

Fig. 5 View of glass tanks and dynamometer

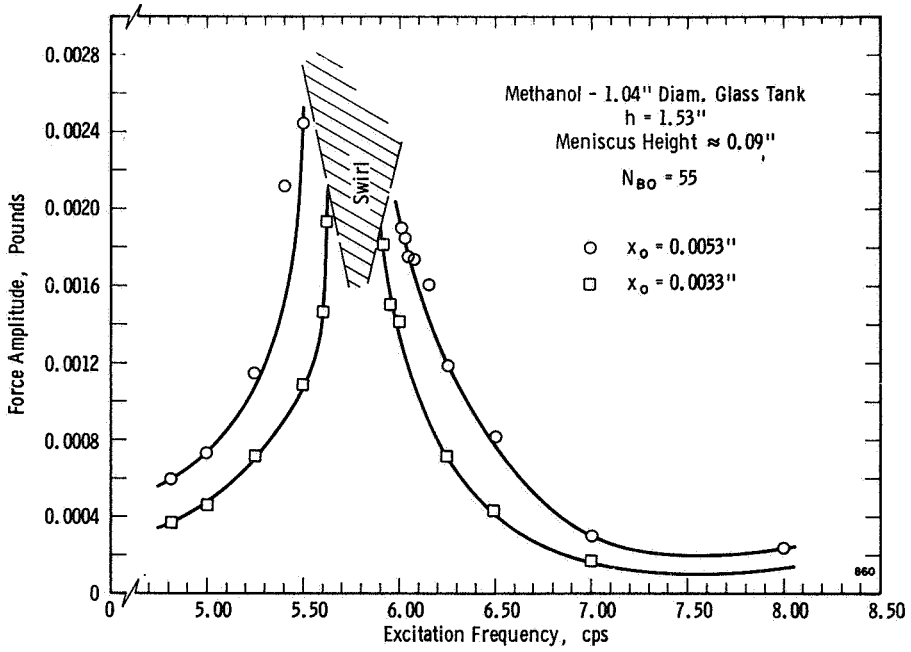

Fig. 6 Force response curve for methanol, Bond number = 55

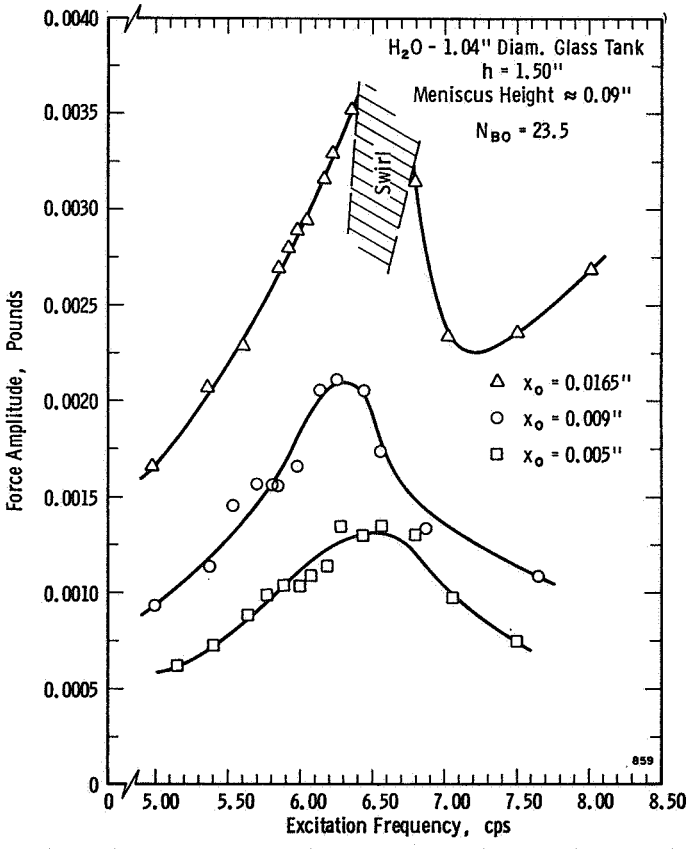

Fig. 7 Force response curve for distilled water, Bond number = 23.5

Four different glass tanks, having diameters ranging from 1.36–0.384 in., were used with three different test liquids: Distilled water, methanol, and carbon tetrachloride. Before each series of tests, the tanks were carefully cleaned in a detergent-and-water solution and rinsed with distilled water. In some of the distilled water tests, the tanks were also cleaned in both a NaOH solution and a hot chromic acid solution. The top of the tank was then covered with a clean plastic wrapper which was removed only to put in the test liquid. The liquids were all reagent grade. In this way, the liquid surface was kept free of contamination.

Figs. 6 and 7 show typical results for methanol and distilled water in a 1.04-in-dia tank. (As nearly as could be determined, the static contact angle of the liquids against the tanks was 0 deg and, except as discussed subsequently, the motion appeared to approximate the "free edge" condition quite well.) The Bond number for the methanol is 55 and, for the water, it is 23.5. The solid lines in these figures are faired curves through the data. There is a pronounced resonance in the methanol curve near 5.75 cps; the curve, in fact, is quite similar to a resonance curve for ordinary high-g sloshing. Near resonance, the sloshing is of the rotary or swirling type encountered in high-g sloshing [13] in which the surface wave rotates around the tank. The shaded areas indicate in a crude fashion the swirl-zone boundaries. Once swirling is encountered, the sloshing force, of course, rotates around the tank also, and thus the forces in this zone cannot be measured nor the exact resonant frequency found.

The water responded in a quite different fashion. The resonance peak is near 6.5 cps instead of the expected value of 5.75 cps. (The theoretical shift in frequency because of the lower N_{BO} of the water is not nearly of this magnitude.) Also, the boundaries of the swirling are displaced upward by a sizable amount and the response curves appear to be heavily damped. Yet, the difference in the viscosity of the water and the methanol (ν_{H_2O} = 1.01 c.s., ν_{meth} = 0.59 c.s.) is not sufficient to explain the variance in the response of the two liquids. Visual observations indicated that the water did not slide freely along the tank walls, even though extreme care was used to prevent contamination of the water and the tanks; as indicated previously, this "sticking" seems to cause additional energy dissipation. Since the interest here is in the "free edge" condition, the response curves for water are not compared to the theoretical predictions.

The experimental value of the natural frequency is determined from the response curves by assuming it is halfway between the swirl boundaries for the lowest excitation amplitude; this is not an exact procedure, but the approximation improves as the width of the swirl region decreases. These values are compared with the present theory in Fig. 8, which also shows the frequency equation of [9]. While there is considerable scatter of the data about the theoretical curve, the general trend of the data and the present theory is in agreement. In fact, except for N_{BO} = 14, the experimental frequencies are below the high-g limit as the theory predicts; and, for several cases, the high-g frequency lies above, i.e., to the right of, the swirl boundaries whereas the true

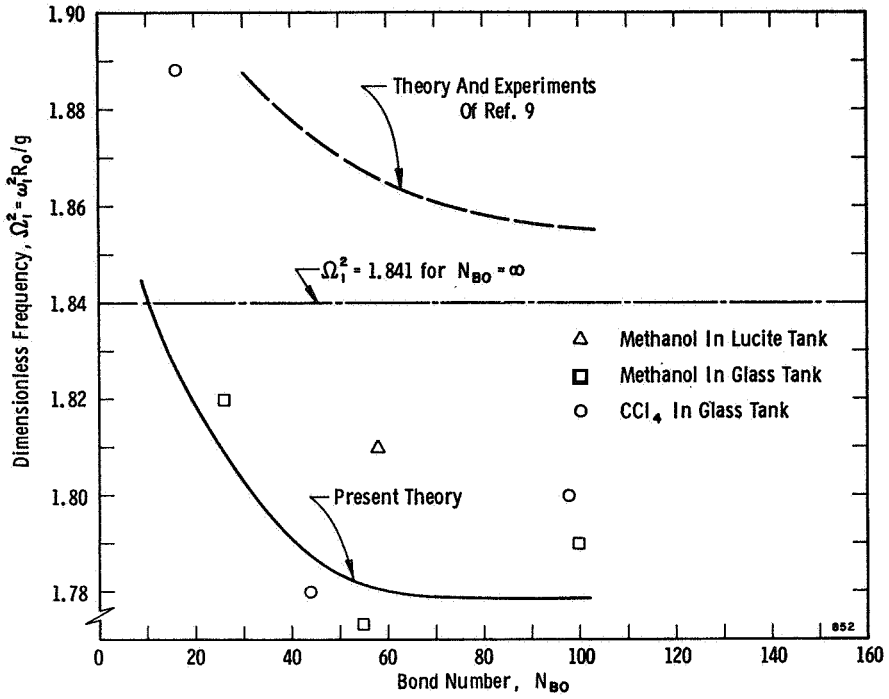

Fig. 8 Comparison of theoretical and experimental natural frequencies for fundamental mode

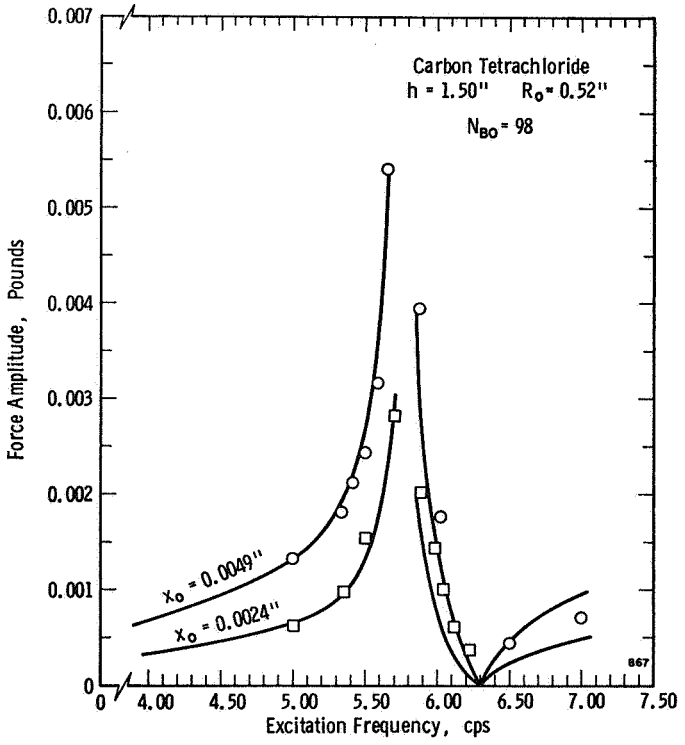

Fig. 9 Comparison of theoretical and experimental force response, $N_{BO} = 98$

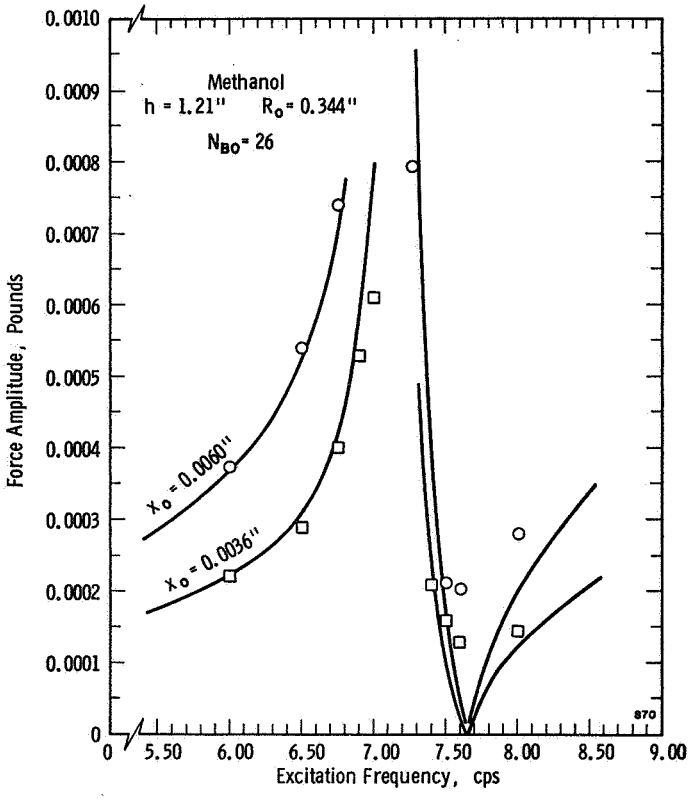

Fig. 10 Comparison of theoretical and experimental force response, $N_{BO} = 26$

natural frequency must lie within the swirl region.

The force response of the proposed mechanical model, with only the fundamental sloshing mass included, is compared with the experimental results in Figs. 9, 10, and 11 for N_{BO} of 98, 26, and 14. (The solid lines in the figures are the theory, and the squares and circles are the experimental data.) The mechanical model and the test results agree very well although there is some discrepancy in the part of the curves above resonance, at least some of which is caused by the influence of higher-order modes neglected in the model. However, for $N_{BO} = 14$ (Fig. 11), there are more serious differences. If the theoretical natural frequency, $f = 9.66$ cps, is used in the model, the predicted forces are generally too large; if the experimental natural frequency, $f = 9.80$ cps, is used, the predicted and the observed forces agree considerably better. It appears, then, that more terms in the velocity potential and wave shape series for $N_{BO} = 14$ need to be retained for proper convergence in the computations.

Conclusions

The analysis shows that the amount of liquid taking part in low-g sloshing is less than that for high-g sloshing. This is a

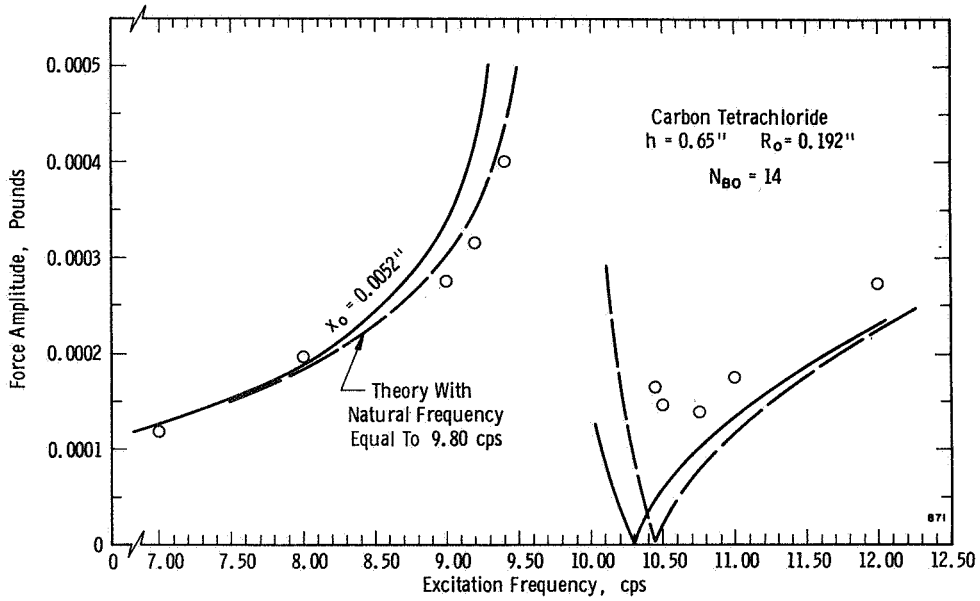

Fig. 11 Comparison of theoretical and experimental force response, N_{BO} = 14

reasonable result because, for the same tank size and the same total amount of contained liquid, more of the liquid is in contact with the walls under low-g conditions; thus more of the liquid must follow the motion of the tank; that is, more of the liquid must be assigned to the rigidly attached mass, m_0, in the mechanical model and less to the sloshing masses. The experimental tests have verified the force response of the proposed mechanical model with about the same degree of accuracy as similar models for high-g sloshing.

The experimental program has demonstrated that it is possible to simulate low-gravity sloshing (i.e., low N_{BO} sloshing) by the use of small models and still get usable results. The amount of damping with such tanks did not appear to be critical. However, care must be used in these kinds of tests to insure that the tanks are very clean and the liquids pure; furthermore, the characteristics of the test liquids and the tank materials should be such as to duplicate the desired conditions of a "free," "partially stuck," or "stuck" contact line.

References

1 Bauer, H. G., "Fluid Oscillations in the Containers of a Space Vehicle and Their Influence Upon Stability," NASA TR R-187, Feb. 1964.

2 Lomen, D. O., "Liquid Propellant Sloshing in Mobile Tanks of Arbitrary Shape," NASA CR-222, Apr. 1965.

3 Abramson, H. N., Chu, W-H., and Dodge, F. T., "Nonlinear Effects in Lateral Sloshing," chapter 3 of *The Dynamic Behavior of Liquids in Moving Containers*, Abramson, H. N., ed., NASA Special Publication SP-106, U. S. Government Printing Office, 1966.

4 Skalak, R., and Yarymovych, M., "Forced Large Amplitude Surface Waves," *Proceedings of the Fourth U. S. National Congress of Applied Mechanics*, ASME, 1962, pp. 1411–1418.

5 Dodge, F. T., Kana, D. D., and Abramson, H. N., "Liquid Surface Oscillations in Longitudinally Excited Rigid Cylindrical Containers," *AIAA Journal*, Vol. 3, No. 4, Apr. 1965, pp. 685–695.

6 Kana, D. D., and Dodge, F. T., "Bubble Behavior in Liquids Contained in Vertically Vibrated Tanks," *Journal of Spacecraft and Rockets*, Vol. 3, No. 5, May 1966, pp. 760–763.

7 Habip, L. M., "On the Mechanics of Liquids in Subgravity," *Astronautica Acta*, Vol. 11, No. 6, 1965, pp. 401–409.

8 Reynolds, W. C., Saad, M. A., and Satterlee, H. M., "Capillary Hydrostatics and Hydrodynamics at Low-G," Technical Report LG-3, Department of Mechanical Engineering, Stanford University, Stanford, Calif., Sept. 1964.

9 Satterlee, H. M., and Reynolds, W. C., "The Dynamics of the Free Liquid Surface in Cylindrical Containers Under Strong Capillary and Weak Gravity Conditions," Technical Report LG-2, Department of Mechanical Engineering, Stanford University, Stanford, Calif., May 1964.

10 Benedikt, E. T., "A Study of Propellant Behavior at Zero Gravity," Final Report, Contract NAS8-11097, North American Aviation, Space and Information Systems Division, Apr. 1966.

11 Ryan, R. S., and Buchanan, H., "An Evaluation of the Low-G Propellant Behavior of a Space Vehicle During Waiting Orbit," NASA TM X-53476, June 1966.

12 Swalley, F. E., Platt, G. K., and Hastings, L. J., "Saturn V Low-Gravity Fluid Mechanics Problems and Their Investigation by Full-Scale Orbital Experiment," *Fluid Mechanics and Heat Transfer Under Low Gravity*, Proceedings of the 1965 Symposium sponsored by USAF-OSR and Lockheed Missiles and Space Co., Cohen, H., and Rogers, M., eds.; no publisher given, pp. 1-1–1-24.

13 Hutton, R. E., "An Investigation of Resonant, Nonlinear Nonplanar Free Surface Oscillations of a Liquid," NASA TN D-1870, May 1963.

14 Miles, J. W., "Damping of Gravity Waves by Surface Films," *Sixth Symposium on Naval Hydrodynamics*, Vol. 2, Paper 23, Washington, D. C., Sept. 1966.

15 Satterlee, H. M., and Chin, J. H., "Meniscus Shape Under Reduced-Gravity Conditions," *Fluid Mechanics and Heat Transfer Under Low Gravity*, Proceedings of the 1965 Symposium sponsored by USAF-OSR and Lockheed Missiles and Space Co., Cohen, H., and Rogers, M., eds.; no publisher given, pp. 13-1–13-24.

16 Dodge, F. T., and Garza, L. E., "Experimental and Theoretical Studies of Liquid Sloshing at Simulated Low Gravities," Technical Report No. 2, Contract NAS8-20290, Southwest Research Institute, San Antonio, Texas, Oct. 1966.

APPENDIX

The constants, or Fourier-Bessel coefficients, in equation (11) and (12) are

$$C1_{nm} = \frac{2\lambda_n^2}{(\lambda_n^2 - 1)[J_1(\lambda_n)]^2} \int_0^1 R \left\{ -\lambda_m J_1(\lambda_m R) + \frac{3\beta R^2}{2(1 - R^3)^{1/2}} J_1'(\lambda_m R) \right\} J_1(\lambda_n R) e^{\lambda_m \beta [1 - (1 - R^3)^{1/2}]} \, dR$$

$$C2_{nm} = \frac{2\lambda_n^2}{(\lambda_n^2 - 1)[J_1(\lambda_n)]^2} \int_0^1 \times R J_1(\lambda_m R) J_1(\lambda_n R) e^{\lambda_m \beta [1 - (1 - R^3)^{3/2}]} \, dR$$

and

$$C3_{nm} = \frac{2\lambda_n^2}{(\lambda_n^2 - 1)[J_1(\lambda_n)]^2} \int_0^1 \frac{R}{(N_{BO})(1 - R^3 + \frac{9}{4}\beta^2 R^4)^{3/2}} \times \left\{ (1 - R^3)^{1/2} \lambda_m^2 J_1(\lambda_m R) + \tfrac{9}{4}\beta^2 R^2 (1 - R^3) J_1(\lambda_m R) + \left[\frac{9\beta^2 R^3 (1 - 0.25R^3)(1 - R^3)^{1/2}}{(1 - R^3 + \frac{9}{4}\beta^2 R^4)^{1/2}} \right] J_1'(\lambda_m R) \right\} J_1(\lambda_n R) dR$$

Reprinted from the September 1967
Journal of Applied Mechanics

SIMULATED LOW-GRAVITY SLOSHING IN CYLINDRICAL TANKS INCLUDING EFFECTS OF DAMPING AND SMALL LIQUID DEPTH

by

Franklin T. Dodge
Luis R. Garza
Senior Research Engineers
Department of Mechanical Sciences
Southwest Research Institute
San Antonio, Texas

ABSTRACT

Liquid sloshing in cylindrical tanks is studied under conditions of simulated low gravities by using small diameter tanks to get surface tension forces comparable in magnitude to the body forces. In the tests, the effects of finite liquid depths and the determination of the smooth wall damping are emphasized. The experimental and theoretical results show that the fluid dynamics are affected by small h/d ratios in much the same way as for normal, large Bond number sloshing. Measurements of the slosh damping indicate that the damping increases as the Bond number decreases, and two correlation equations for the damping factor are proposed. An equivalent mechanical model developed previously is extended to include h/d variations and linear viscous damping. Comparisons of the force response predicted by the model to that measured in the tests verify the model to a high degree of confidence.

INTRODUCTION

The sloshing of the liquid fuel contained in a space system can strongly affect the performance of the system. During launch and powered flight, the liquid fuel is acted upon by strong body forces, but, during orbital coasting or in deep space, the body forces or "gravity" forces are reduced substantially, and the liquid motion is governed by other, primarily surface, forces. Sloshing under these conditions is usually called "low-g" sloshing or, more exactly, "low Bond number" sloshing.

Because of the lack of a convenient low gravity laboratory, not much data exist concerning low-g sloshing. Habip [1]* has reviewed most of the pertinent work done prior to 1965, and, recently, Yeh [2] and Chu [3] have studied analytically low-g sloshing in axisymmetric tanks; however, no numerical examples were given. As part of a study of the Apollo spacecraft propulsion system, a number of approximate analyses of low-g liquid motions, such as reorientation, ullage gas entrainment, and sloshing have been formulated [4], but these analyses pertain to nearly zero gravity, a regime where almost no experimental data are available for verification of the analyses. In work reported previously by us [5], an experimental and theoretical study of moderately low-g sloshing was conducted. The slosh force data given in [5] were the first such data, apparently, ever collected under low Bond number conditions

*Numbers in brackets denote references.

Reprinted from PROCEEDINGS OF THE 1968 HEAT TRANSFER AND FLUID MECHANICS INSTITUTE, Ashley F. Emery and Creighton A. Depew, Editors. Stanford University Press, 1968;

and, except for the present tests, are still the only existing force measurements. The experimental results were obtained by simulating low gravity through the use of small diameter tanks; in this way, the ratio of gravity forces to surface tension forces (the Bond number, N_{BO}) could be made equal to values of N_{BO} expected in, for example, orbital coasting of Saturn-class boosters. Clark and Stephens [6] also obtained data on low-g slosh damping and natural frequency by this same method. Other experimental results have been gathered by free-fall tests in "drop towers" [7, 8]. All of these results, in general, are for specialized tank geometries or situations, and no theory has yet been able to explain completely the dynamics of low-g sloshing throughout the range from true zero-gravity (zero Bond number) to normal or high gravity (large Bond numbers).

The purpose of the work reported here was to extend the research described in [5] to include the effects of small liquid height-to-tank diameter ratios and to determine the magnitude of viscous damping under small Bond number conditions. Improvements in the experimental apparatus allowed better and more complete measurements to be made than these reported in [5]. Likewise, modifications and improvements in the theory now show that the theory is in excellent agreement throughout the range of Bond numbers tested.

EXPERIMENTAL APPARATUS AND PROCEDURE

With two major exceptions, the experimental setup used in the present tests was similar to that described in Ref. [5]. First, instead of attaching the small dynamometer package directly to the armature of an 1100-lb electromagnetic shaker, the experimental package was attached to a massive horizontal shake table which was then excited in pure translation by a much smaller, 50-lb output electromagnetic shaker. The dynamometer package (without its protective cover) is shown attached to the shake table in Fig. 1; the tank on the left, with an inverted ellipsoidal bottom, is one used in other tests. Because of the linear ball bearings guiding the shake table and the general ruggedness of the supports, an excellent sinusoidal excitation signal, with little out-of-plane motion, was obtained. * This improvement, and an improvement in the electronic amplification system of the slosh force signal, allowed sufficiently small excitation amplitudes to be used to sweep completely through the slosh resonance frequency without encountering swirling motion of the liquid. Thus, slosh damping factors could be obtained by the usual half-bandwidth technique. Second, a carbon film potentiometer was attached directly to the support frame; this allowed a continuous monitoring of the displacement amplitude with a consequent large improvement in the accuracy of the data.

The experimental procedures, calibrations, and data reductions were the same as reported previously [5]. Briefly, however, two tanks are used for each test; one tank, empty, and called the balance tank, is used to cancel the inertia of the other tank, containing the test liquid and called the active tank, so that the residual force felt by the dynamometer when the active tank is empty is very small. The sloshing force is detected by semiconductor strain gages (gage factor = 118) mounted on the tension-compression arms of the dynamometer; the output of the gages is amplified and recorded on an

*The shake table is described in [9].

oscillograph. The excitation frequency, which could be maintained to the fourth significant figure of the period (in seconds), is determined with a digital period counter.

Three different liquids (carbon tetrachloride, methanol, and acetone) were used in four different tanks (diameters: 1.36 in., 1.04 in., 0.688 in., and 0.383 in.). The variation in tank diameter and liquid properties was sufficient to cover a range of N_{BO} from 14 to 175.

TEST RESULTS

There were two main objectives of the experimental program: (1) measure the lateral slosh force for the fundamental mode as a function of the excitation frequency and amplitude, and (2) measure the slosh damping present. The parameters to be varied were the Bond number and the liquid depth.

All of the tests were run with glass tanks and reagent grade liquids. As nearly as could be determined visually, the contact angle was zero degrees for all the liquids against the tank walls, and the sloshing motion of the liquids appeared to approximate the "free edge" or no contact angle hysteresis condition very well.

Slosh Force Response and Resonant Frequency

Figures 2 through 4 show some typical force response curves for $CC\ell_4$ and methanol. The solid lines in these figures are faired curves through the experimental data. To facilitate direct comparisons, neither the force nor the frequency is nondimensionalized in any way. Note that the combination of small excitation amplitudes, very little out-of-plane motion of the shake table, and the natural slosh damping allowed complete resonance curves to be obtained; that is, no liquid swirling or rotation was evident.

As mentioned previously, the range of N_{BO} was from 175 ($CC\ell_4$ in 1.36-in. tank) to 14 ($CC\ell_4$ in 0.383-in. tank). The range of the ratio of liquid depth to tank diameter used in the tests was from 1.25 to 0.25; even larger h/d ratios were used in some tests, but these results were substantially the same as for h/d = 1.00 or 1.25.* Other information given in the figures includes the amplitude of tank excitation (x_o), the resonant frequency (f_1) as determined by the peak in the response curve, the slosh damping coefficient (γ_s) as determined by the half-bandwidth technique, and the wave height (δ) at resonance.

By comparing the resonant frequency, f_1, to that calculated by theoretical results for the undamped natural frequency at large Bond numbers [i.e., $2\pi f_1 = \left\{3.682\ (g/d)\ \tanh\ 3.682\ (h/d)\right\}^{1/2}$], it can be seen that the resonant frequency for N_{BO} = 175 is slightly lower than the corresponding high-g frequency for the same h and d. As the Bond number is decreased, however, the resonant frequency increases rapidly above the high-g frequency. This is similar to the results presented in [5], which have been confirmed by Clark and

*The depth of liquid below the bottom of the curved meniscus is used in computing h/d. The average liquid depth is larger than h by an amount 0.132 βd where β is the root of $\beta^3 N_{BO} - \beta^2 - 2/3 = 0$ [5]; this is only an approximate calculation, although fairly accurate; a great amount of exact numerical work is also available [14].

Stephens [6]; however, other analytical results imply that the low Bond number natural frequency should never fall below the high-g frequency [15]. In any event, the change in natural frequency throughout the range of N_{BO}'s greater than 10 is less than about 10%.

Some slight nonlinearity is evident in the force-response curves, especially for the smaller h/d ratios or for the larger γ_s's. Qualitatively, however, the force response even for the smallest N_{BO} of 14 is similar to ordinary large Bond number sloshing.

Slosh Damping

For each resonant force response curve, the equivalent viscous damping present in the sloshing was computed by the half-bandwidth technique. The resulting damping coefficients, γ_s (γ_s is defined as the ratio of the apparent damping to the critical damping and is equivalent to the logarithmic decrement divided by 2π), for $h/d \geq 1.0$ are shown graphically in Fig. 5. (For smaller h/d, γ_s varies with the liquid depth, but no change in damping was apparent for $h/d \geq 1.0$; this agrees with high Bond number results.) The abscissa in Fig. 5 is $N_{GA}^{-1/2}$, N_{GA} being the Galileo number, a form of the Reynolds number pertinent to high Bond number sloshing. Although N_{GA} is usually defined as $g^{1/2}R_o^{3/2}\nu^{-1}$, it is clear on both dimensional and theoretical grounds that "g" really enters by way of the natural frequency [i.e., $f_1 \propto (g/R_o)^{1/2}$ when $N_{BO} = \infty$]. Thus, for very small N_{BO}'s, the g should be eliminated from N_{GA}, and it should be redefined in terms of natural frequency; here, however, f_1 is almost proportional to $g^{1/2}$ (for $N_{BO} > 10$), so the usual definition of N_{GA} is retained.

Both experiment [10] and theory [11] have shown that γ_s is directly proportional to $N_{GA}^{-1/2}$ for large Bond number conditions. The data included in Fig. 6 also show this since a large N_{BO} corresponds to a small N_{GA} on this plot. But, for small N_{BO} (large $N_{GA}^{-1/2}$), γ_s is considerably larger than that predicted by the usual correlation equation $\gamma_s = 0.83\, N_{GA}^{-1/2}$, which is valid for large N_{BO}'s. Other experimenters have also observed the increase in γ_s [6, 12]. On a purely empirical basis, Keulegan [12] and Clark and Stephens [6] concluded that γ_s should be calculated as the sum of two parts:

$$\gamma_s = \gamma_{N_{GA}} + \gamma_{N_{BO}} \tag{1}$$

where $\gamma_{N_{GA}}$ is a function only of the Galileo number and $\gamma_{N_{BO}}$ only of the Bond number; furthermore, $\gamma_{N_{BO}} \to 0$ as $N_{BO} \to \infty$. Clark and Stephens [6] were able to correlate their data (which are the ○ and □ points in Fig. 6) in this way by using the equation

$$\gamma_s = 0.83\, N_{GA}^{-1/2} + 0.096\, N_{BO}^{-3/5} \tag{2}$$

which reduces to the correct relation as $N_{BO} \to \infty$ but predicts that $\gamma_s \to \infty$ as $N_{BO} \to 0$. In the range tested by them ($8 < N_{BO} < 1000$), Eq. (2) gave a very close fit to their data, although Keulegan in his work with rectangular tanks [11] found that $\gamma_{N_{BO}}$ should vary as N_{BO}^{-1}. To check Eq. (2), the present data were tested against it, as shown in Fig. 6. The correlation is fairly good although not so good as the same equation with Clark and Stephens' original data. Part

of the discrepancy may arise from the fact that the damping in [6] was based on the log decrement of the free decay of the sloshing wave, while the present damping results were based on forced response measurements; free decay tests and forced response tests are equivalent for linear systems, but this may not be true for slightly nonlinear systems such as these.

Neither Keulegan [12] nor Clark and Stephens [5] attempted an explanation of the physics behind the evident variation of γ_s with N_{BO}; in fact, it is not apparent why γ_s should vary independently with N_{BO} since no energy dissipation is provided by surface tension forces alone. J. W. Miles [13] has, however, analyzed the damping of surface waves in tanks by using various approximations to the dissipation provided by viscosity, by diffusion from the bulk liquid to the surface and vice versa during the stretching and contracting of the free surface when it oscillates, by soluble or insoluble films or contaminants on the free surface, and by contact angle hysteresis. He proposed γ_s should be calculated as

$$\gamma_s = \gamma_{N_{GA}}(1 + \gamma_s') + \gamma_L \tag{3}$$

γ_s' is a parameter dependent upon surface properties and for insoluble surface films (in which the variation of the surface tension as the surface stretches is proportional to the undisturbed surface tension), it depends only on a parameter ξ:

$$\gamma_s' = \frac{\xi^2}{(\xi - 1)^2} \tag{4}$$

where

$$\xi \propto \frac{1}{N_{GA}} \left(\frac{gR_o}{f_1^2 N_{BO}} \right) \tag{5}$$

The third term, γ_L, is the contribution to the damping by contact angle hysteresis. According to Miles, both the advance and recession of the meniscus are opposed by constant forces that depend only on the material properties of the liquid-gas-tank interface. He showed that

$$\gamma_L = \frac{\kappa f(N_{BO})}{\delta} \tag{6}$$

where $f(N_{BO})$ depends only on N_{BO}, κ is the magnitude of the constant opposing force, and δ is the wave amplitude. For the present tests, γ_L should be very small (i.e., $\kappa \approx 0$) since no contact angle hysteresis was observed; furthermore, the data of [6] indicate no variation of γ_s with δ although some slight variation is evident in our results. For these reasons, a correlation of the form

$$\gamma_s = 0.83\, N_{GA}^{-1/2} (1 + A N_{BO}^n) \tag{7}$$

was attempted, which is in qualitative agreement with Miles' predicted form for the damping when γ_L is neglected. Results are shown in Fig. 7. The best fit to the data was obtained with A = 8.20 and n = -3/5 so that the correlation equation is:

$$\gamma_s = 0.83\, N_{GA}^{-1/2} \left(1 + 8.20\, N_{BO}^{-3/5}\right) \tag{8}$$

which gives a reasonably good correlation to both the present data and the data of [6].

Equation (8) has the merit that it shows that the energy dissipation arises through the viscosity; however, neither Eqs. (8) nor (2) can be correct for $N_{BO} = 0$ since both predict that $\gamma_s \to \infty$ as $N_{BO} \to 0$ while the experimental results obtained by Salzman, et al. [7], for $N_{BO} \approx 0$ using a drop tower indicate that $\gamma_s = 3.84\, N_{GA}^{-1/2}$.

For $h/d < 1.0$, the trend of the damping data is an increase in γ_s as h/d decreases. This is similar to the variation obtained for large Bond numbers, namely:

$$\gamma_s = 0.83\, N_{GA}^{-1/2} \tanh 1.84\, \frac{h}{R_o} \left[1 + 2\left(1 - \frac{h}{R_o}\right) \operatorname{csch} 3.68\, \frac{h}{R_o}\right]$$

However, for the smallest N_{BO} of 14, γ_s appears to decrease slightly as h/d decreases. For this reason, and because the amount of data collected is not sufficient to predict with any confidence the variation of γ_s with both h/d and N_{BO}, a correlation equation involving h/d has not been attempted.

COMPARISON OF THEORY AND EXPERIMENT

For normal and high-g conditions, an equivalent mechanical model composed of masses, springs, and dashpots gives a very good representation of the force response characteristics of sloshing. Further, it was shown in [5] that the same kind of model, even without damping (dashpots), gives a fairly good representation of low Bond number sloshing. The model developed in [5], however, was limited to $h/d > 1$, no damping, zero degree contact angle, and a "free edge" or no contact angle hysteresis condition. Thus, in this report, the same theoretical model is extended to include linear viscous damping and any value of h/d. The zero degree contact angle and no hysteresis conditions are retained since these seem to be the most practical cases. To modify the theory, it is necessary to use a velocity potential which allows for finite liquid depth; this can be done by replacing $\exp(\lambda_n z)$ in Eq. (19) of [5] by $\cosh \lambda_n z + \tanh \lambda_n h/R_o \sinh \lambda_n z$ and then proceeding as outlined in [5]. The details are not given here. The linear viscous damping is added after the fact by modifying the force response equations.

For the proposed model, consisting of one mass, m_o, attached rigidly to the tank and one mass, m_1, attached to the tank through a spring (spring constant k_1) and dashpot (damping coefficient γ_s), the amplitude of the force response for simple harmonic excitation of frequency f is

$$F = 4\pi^2 (m_o + m_1) x_o f^2 \left\{1 + \frac{m_1}{m_o + m_1}\left[\frac{(f/f_1)^2}{1 - (f/f_1)^2 + 2i\gamma_s (f/f_1)}\right]\right\} \tag{9}$$

where $i = \sqrt{-1}$. The parameters f_1 and m_1 ($k_1 = 4\pi^2 f_1^2 m_1$) as calculated by the present theory are shown in Figs. 8 and 9. All of the parameters are given as

multiples of the corresponding high-g quantity calculated for the same R_o, h/d, g, and m_T ($m_T = m_o + m_1$ is the total mass of liquid contained in the tank); for reference, these high-g quantities are

$$f_1 = \frac{1}{2\pi}\left\{1.841\ \frac{g}{R_o}\ \tanh 3.682\ \frac{h}{d}\right\}^{1/2}$$

$$m_1 = 0.227 m_T \left(\frac{d}{h}\right) \tanh 3.682\ \frac{h}{d} \qquad (10)$$

The low-g frequency and slosh mass for h/d = 1.0 shown in the figures differ somewhat from the results presented in [5]; the difference is caused by retaining more terms here in the infinite series used to compute the model parameters.

By using the figures to calculate f_1, m_1, k_1, and $m_o = m_T - m$, the force response for any N_{BO} and h/d can be determined. Comparisons of the force response predicted by the mechanical model to our experimental results are shown in Figs. 10, 11, and 12; the value of γ_s used in Eq. (9) to compute the force corresponds to the experimental tests for the indicated x_o, R_o, h/d, and liquid. The comparison throughout the N_{BO} and h/d range is uniformly good, as can be seen. The darkened triangle (▼) along the frequency axis in each plot is the theoretical undamped natural frequency, f_1, whereas the peak in the resonance curve locates the damped resonant frequency; the difference between the two is entirely due to the damping.

Considering the good correlation between the frequency of the theoretical peak force and the experimental peak, it may be concluded that the curves in Fig. 8 adequately predict the low-g slosh frequency. Likewise, since the peak force for the theory and experiment are very close, the slosh mass m_1 is given adequately by Fig. 9.* Thus, the proposed mechanical model gives a good representation of the low-g sloshing dynamics.

CONCLUSIONS

The experimental tests have verified that the use of small diameter tanks is adequate to simulate moderately low Bond number sloshing, including h/d variations and the effects of damping.

The smooth-wall damping coefficient was shown to increase as the Bond number decreased; for $N_{BO} > 10$, an adequate correlation of the damping coefficient is provided by either

$$\gamma_s = 0.83\ N_{GA}^{-1/2} + 0.096\ N_{BO}^{-1/2}$$

or

$$\gamma_s = 0.83\ N_{GA}^{-1/2}\left(1 + 8.20\ N_{BO}^{-3/5}\right)$$

The second equation has the virtue of being in qualitative agreement with

*The peak force depends almost entirely on only m_1 and γ_s.

existing theories, but neither correlation equation can be extended much below $N_{BO} = 10$.

The experiments, in conjunction with the theory, show that the low Bond number slosh mass, natural frequency, and spring constant all decrease more slowly as h/d decreases than do the corresponding high Bond number quantities. In other words, if the low Bond number parameters decreased at the same rate as did the high Bond number parameters, all of the frequency curves in Fig. 8, for example, would be parallel, and, in fact, all the curves would collapse onto the h/d = 1.0 curve. Since the smaller h/d curves are translated upward and moreover spread apart as N_{BO} decreases, it can be concluded that the frequency decreases less slowly with h/d than does tanh 3.682 h/d, which is the rate of decrease for large Bond number conditions.

Comparisons of the force response predicted by the theoretical model with the actual test values verify the mechanical model to about the same degree of confidence as similar models for high Bond number sloshing. The comparisons also show the importance of accounting for the damping in making natural frequency determinations; for example, with $CC\ell_4$ in a 0.383-in. diameter tank, the actual resonant frequency is about 9.7 cps (for h/d = 1.0), whereas the undamped theoretical natural frequency is 9.95 cps. (The resonant frequency for the mechanical model is less than the natural frequency by the factor $\sqrt{1-2\gamma_s^2}$.)

ACKNOWLEDGEMENTS

The research presented herein was sponsored by NASA-Marshall Space Flight Center under Contract NAS8-20290.

NOMENCLATURE

Symbol

- d - diameter of tank
- f - frequency of tank excitation
- f_1 - natural frequency or resonant frequency of sloshing
- g - acceleration of gravity or equivalent linear acceleration
- h - depth of liquid below bottom of meniscus
- k_1 - spring constant in mechanical model
- m_1 - slosh mass in mechanical model
- m_o - rigidly attached mass in mechanical model
- m_T - $m_o + m_1$, total liquid mass
- N_{BO} - Bond number, $\rho g R_o^2/T$ where ρ and T are liquid density and surface tension.
- N_{GA} - Galileo number, $(gR_o^3/\nu^2)^{1/2}$

R_o - tank radius

x_o - amplitude of tank excitation

γ_s - slosh damping coefficient

δ - amplitude of slosh wave

ν - kinematic viscosity

LIST OF REFERENCES

1. Habip, L. M. On the Mechanics of Liquids in Subgravity, Astronautica Acta, 11, No. 6, pp. 401-409 (1965).

2. Yeh, G. C. K. Free and Forced Oscillations of a Liquid in an Axisymmetric Tank at Low-Gravity Environments, Trans. ASME, J. Applied Mech., 34, Series E, No. 1, pp. 23-28, March 1967.

3. Chu, W. H. Low Gravity Liquid Sloshing in an Arbitrary Axisymmetric Tank Performing Translational Oscillations. Technical Report No. 4, Contract NAS8-20290, Southwest Research Institute, San Antonio, Texas, March 1967.

4. Hollister, M. P., Satterlee, H. M., and Cohan, H. A Study of Liquid Propellant Behavior during Periods of Varying Accelerations. Final Report, Contract No. NAS9-5174, Lockheed Missiles and Space Company, Sunnyvale, California, June 1967.

5. Dodge, F. T., and Garza, L. R. Experimental and Theoretical Studies of Liquid Sloshing at Simulated Low Gravities, Trans. ASME, J. Applied Mech., 34, Series E, No. 3, pp. 555-562, September 1967.

6. Clark, L. V., and Stephens, D. G. Simulation and Scaling of Low-Gravity Slosh Frequencies and Damping. AIAA Space Simulation Symposium Preprint, Philadelphia, Pennsylvania, September 1967.

7. Siegert, C. E., Petrash, D. A., and Otto, E. W. "Time Response of Liquid-Vapor Interface after Entering Weightlessness," NASA TN D-2458 (1964).

8. Salzman, J. A., Labus, T. L., and Masica, W. J. "An Experimental Investigation of the Frequency and Viscous Damping of Liquids during Weightlessness," NASA D-4132 (1967).

9. Abramson, H. N., Chu, W. H., and Kana, D. D. Some Studies of Nonlinear Lateral Sloshing in Rigid Containers, Trans. ASME, J. Applied Mechanics, 33, Series E, No. 4, pp. 777-784, December 1966.

10. Stephens, D. G., Leonard, H. W., and Perry, T. W. "Investigation of the Damping of Liquids in Right-Circular Cylinders, Including the Effects of a Time Variant Liquid Depth," NASA TN D-1367 (1962).

11. Case, K. M., and Parkinson, W. C. Damping of Surface Waves in an Incompressible Liquid, J. Fluid Mech., 2, pp. 172-184, March 1967.

12. Keulegan, G. H. Energy Dissipation in Standing Waves in Rectangular Basins, J. Fluid Mech., 6, pp. 33-50, July 1959.

13. Miles, J. W. Surface Wave Damping in Closed Basins, Proc. Royal Society (London), 297 A, No. 1451, pp. 459-475, March 1967.

14. Bashforth, F., and Adams, J. C.: An Attempt to Test the Theories of Capillary Action. University Press, Cambridge, England, 1883.

15. Concus, P., Crane, G. E., and Satterlee, H. M.: Small Amplitude Lateral Sloshing in a Cylindrical Tank with a Hemispherical Bottom Under Low Gravitational Conditions. NASA CR-54700, Jan. 1967.

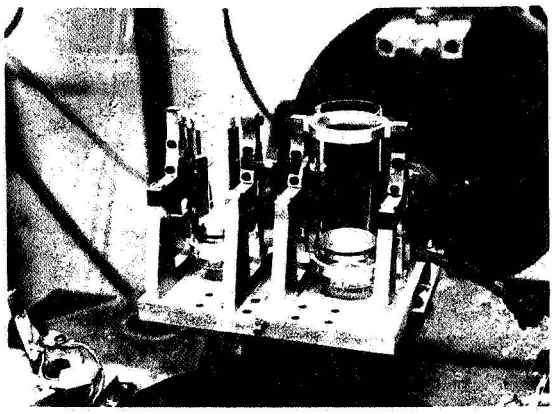

FIG. 1. Dynamometer Package on Shake Table

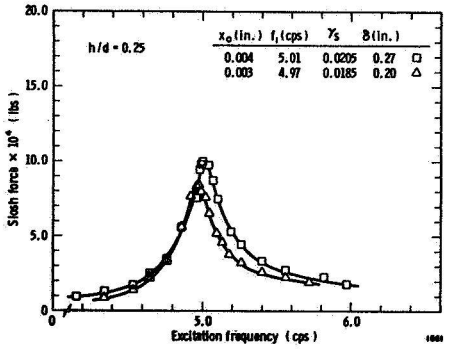

FIG. 2. Response Curves for Methanol in 1.04" Diameter Tank, N_{BO} = 60

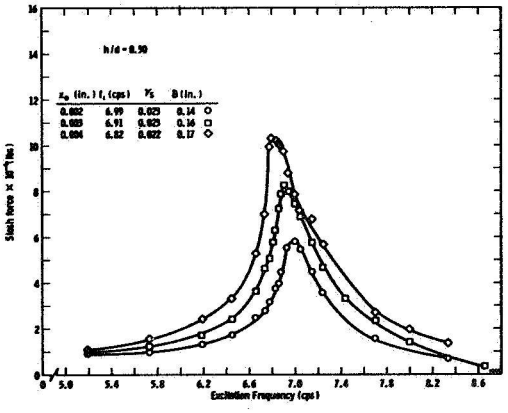

FIG. 3. Response Curves for $CC\ell_4$ in 0.688" Diameter Tank, N_{BO} = 45

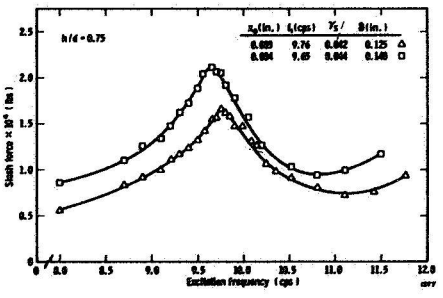

FIG. 4. Response Curves for $CC\ell_4$ in 0.383" Diameter Tank, N_{BO} = 14

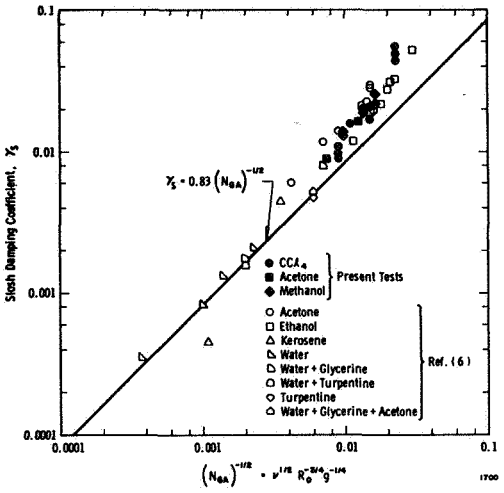

FIG. 5. Variation of Smooth Wall Damping Coefficient with Galileo Number

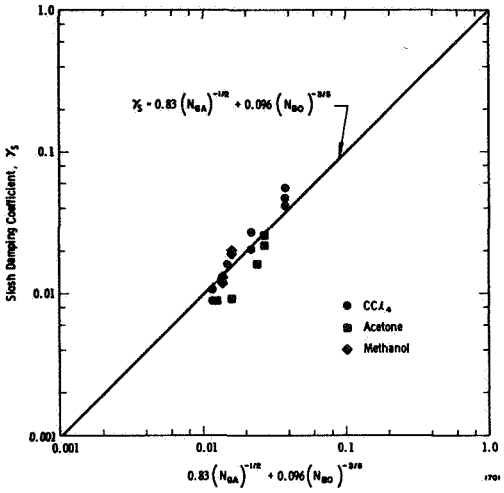

FIG. 6. Variation of γ_s with Correlation Equation of Clark and Stephens [6]

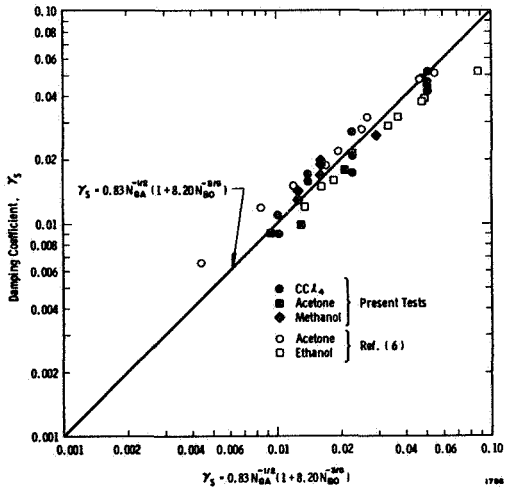

FIG. 7. Variation of γ_s with Present Correlation Equation

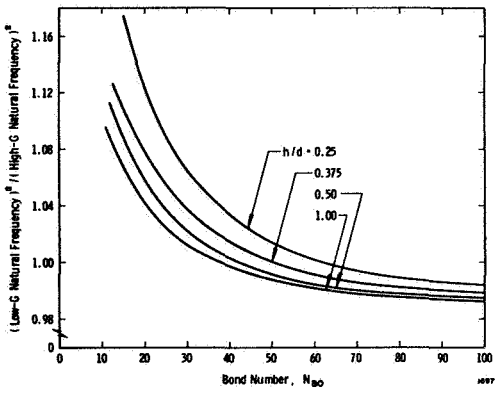

FIG. 8. Variation of Slosh Natural Frequency with Bond Number

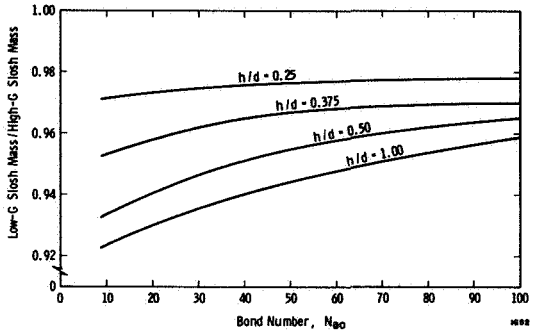

FIG. 9. Variation of Slosh Mass with Bond Number

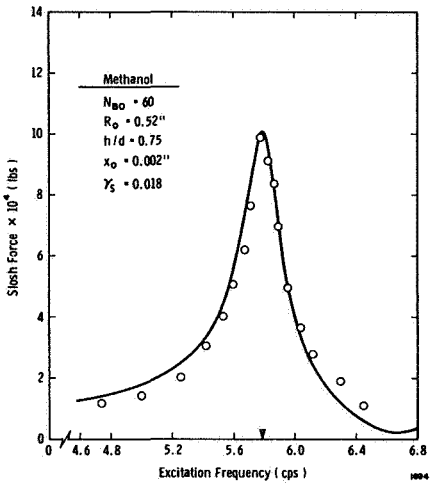

FIG. 10. Comparison of Theory and Experiment, $N_{BO} = 60$

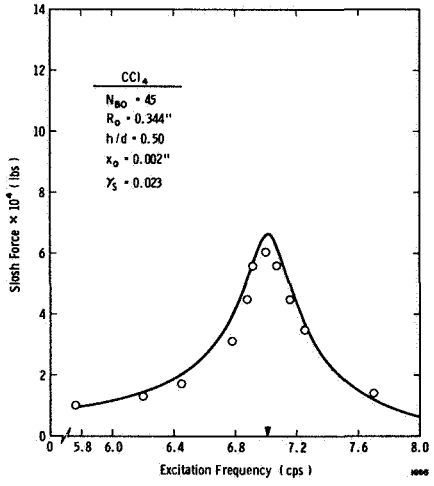

FIG. 11. Comparison of Theory and Experiment, $N_{BO} = 45$

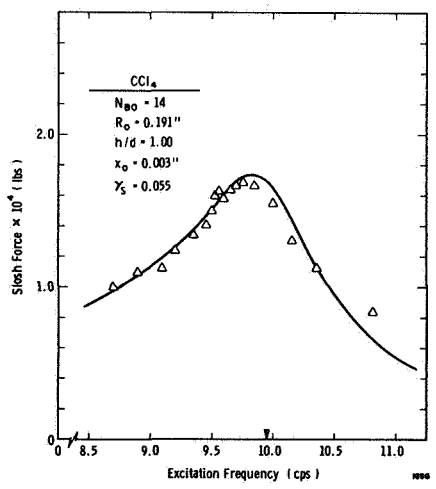

FIG. 12. Comparison of Theory and Experiment, $N_{BO} = 14$

Simulated Low-Gravity Sloshing in Spherical, Ellipsoidal, and Cylindrical Tanks

FRANKLIN T. DODGE* AND LUIS R. GARZA†
Southwest Research Institute, San Antonio, Texas

Nomenclature

f_1 = first mode slosh natural frequency
g = gravity or equivalent linear axial acceleration
N_{BO} = Bond number, $\rho g R_o^2/\sigma$
R_o = radius of tank
ν, ρ = liquid kinematic viscosity and density
σ = surface tension

Introduction

SINCE the primary effect of reduced gravity on propellant sloshing is to accentuate the surface tension forces relative to the gravity forces in the body of the liquid, the Bond number, $N_{BO} = \rho g R_o^2/\sigma$, which is a measure of these two forces, is the correct indicator of "low-gravity" simulation. ($N_{BO} = 0$ indicates zero gravity, but $N_{BO} = 40$ is typical for large boosters even when gravity is only 10^{-5} of earth gravity.) Also, for $N_{BO} < 100$ simulations, the correct static contact contact angle of the free surface at the tank walls must be duplicated and contact angle "hysteresis" or "dynamic contact angle" accounted for.

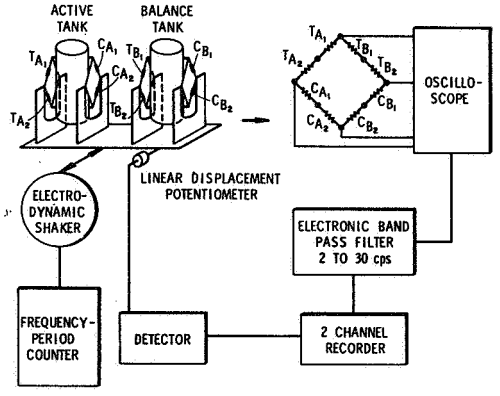

Fig. 1 Schemetic of slosh-force dynamometer.

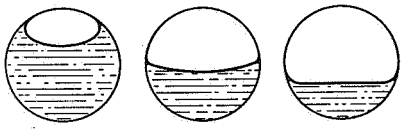

Fig. 2 Change in free-surface curvature with filling level, for equal bond numbers.

Several methods of simulating low gravity using scale models have been advanced. In a *drop-tower*, the effective gravity acting on the liquid is reduced by allowing the experimental package to fall freely, see Ref. 1. In the *magneto-hydrodynamic* method, body forces generated in an electrically conducting liquid by crossed electric and magnetic fields are used to cancel gravity.[2] The *dielectrophoretic* method uses a strong electric field and a dielectric liquid to create body forces opposed to gravity.[2] The *magnetic fluid* method uses a specially prepared magnetic liquid and an axial magnetic field to cancel the gravitational forces.[2]

Most existing steady-state data have been obtained by using *ultra-small models*, see Ref. 3, since surface tension forces can be increased by decreasing the tank diameter. The two main difficulties of this simulation are 1) the small dynamic slosh force is difficult to measure, and 2) the viscous damping is large compared to the prototype; these difficulties generally limit the simulation to $N_{BO} > 10$, which, however, still includes most low-gravity missions to date. The data presented in this Note were obtained by this technique, which requires an extremely sensitive and accurate dynamometer-excitation system. (Slosh forces as small as 0.0005 lb had to be measured during tests.) In principle, the dynamometer-excitation package was similar to but much more sensitive than that used for much larger tanks. The force-measuring system is shown schematically in Fig. 1. Each sensing ele-

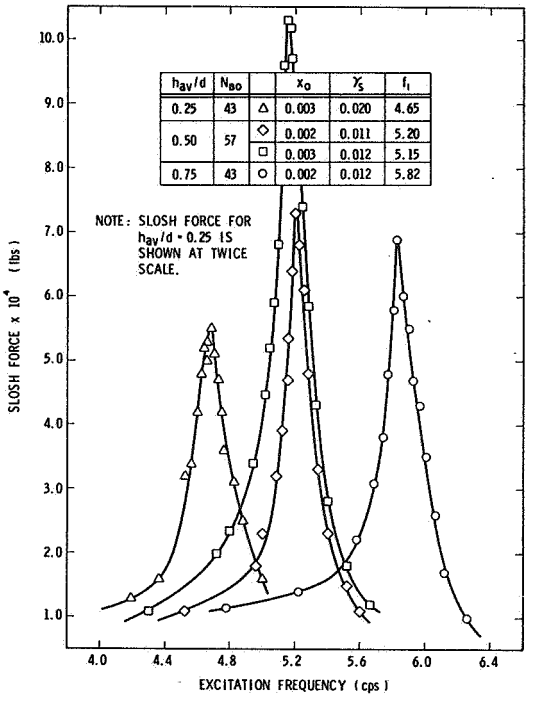

Fig. 3 Typical force response for spherical tanks.

Presented as Paper 69-1004 at the AIAA/ASTM/IES 4th Space Simulation Conference, Los Angeles, Calif., September 8–10, 1969; submitted September 9, 1969; revision received October 24, 1969. Research sponsored by NASA-MSFC Contract NAS8-20290; this Note is a condensation of Technical Reports 6 and 7. The authors express their thanks to G. L. Dugger for his aid in editing the manuscript.

* Senior Research Engineer, Department of Mechanical Sciences. Member AIAA.

† Senior Research Engineer, Department of Mechanical Sciences.

Reprinted from JOURNAL OF SPACECRAFT AND ROCKETS, Vol. 7, No. 2, February 1970, pp. 204-206

ment (a tension-compression link) had bonded to it a semiconductor strain gage (gage factor = 118), and the test tanks were connected directly to the sensing links. The "active tank" contained the test liquid; a duplicate "balance tank" was used to electrically cancel the inertia signal of the empty active tank in a Wheatstone bridge circuit when both tanks were vibrated at the same frequency and amplitude. Thus, during sloshing, the signal recorded was due solely to the sloshing pressures on the tank walls. This procedure improved the sensitivity of the apparatus so greatly that the entire apparatus had to be covered to prevent stray air currents from impinging on the tank and overwhelming the slosh signal.

All the tanks were carefully cleaned before using. Triply distilled water was first used as the test liquid, because of water's high ratio of surface tension to density. But no matter how careful the cleaning, the water's free surface would soon "stick" to the tank walls, and most of the wave action would cease. Since the liquid sliding freely up and down the tank walls (the "free-edge" condition) is the practical case, the tests with water were abandoned and reagent-grade methanol, acetone, and carbon tetrachloride, which are all good cleaners, were used instead; all these liquids had a 0° static contact angle, and no "hysteresis" effects were evident.

By analyzing the errors and inaccuracies in the apparatus and test procedure, the slosh force data were estimated to be within ±5% of their true values.[4]

Test Results

The three experimental objectives were the determination of 1) slosh force amplitude as a function of lateral excitation 2) resonant slosh frequency, and 3) slosh damping. Four tank geometries were employed: flat-bottomed cylindrical (diameters of 1.36, 1.04, 0.688, and 0.383 in.); spherical (diameters of 1.36 and 1.04 in.); and two kinds of oblate ellipsoidal, one having a major-to-minor axis ratio of $(2)^{1/2}/1.0$ (major diameters of 1.354 and 0.760 in.) and the other having a ratio of 1.99/1.0 (the same major diameters). Besides tank geometry, the variables included ρ, σ, ν, and liquid filling level, which thus varied N_{BO} and the Galileo number, $N_{GA} = R_o^{3/2} g^{1/2}/\nu$, the form of Reynolds number pertinent to sloshing.

Cylindrical tanks

These results have been presented elsewhere[4,5] but are reviewed here to point out three important facts. First, the excellent correlation between theory and test helps prove that the simulation method is indeed valid. Secondly, the slosh resonant frequency for $N_{BO} > 10$ is not a strong function of

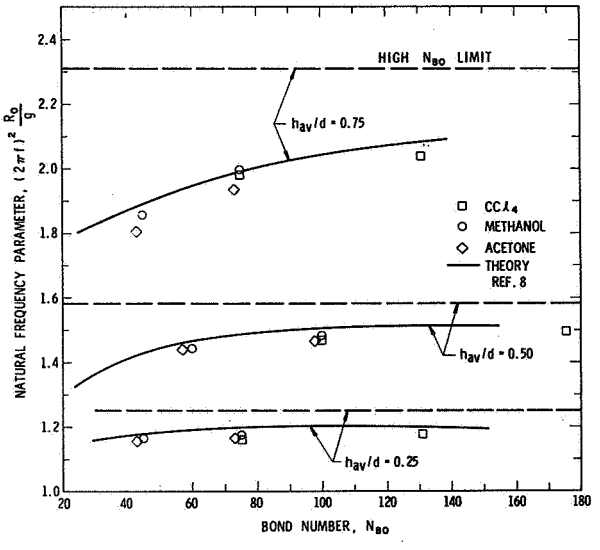

Fig. 4 Variation of natural frequency with bond number for spherical tanks.

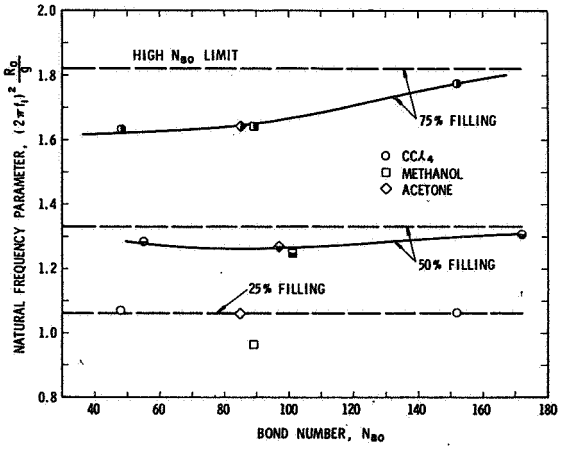

Fig. 5 Variation of natural frequency with bond number for $(2)^{1/2}/1.0$ ellipsoidal tanks.

N_{BO}: the maximum variation in $(2\pi f_1)^2 R_o/g$ is no more than about 10% from $N_{BO} = \infty$ to $N_{BO} = 10$. Thirdly, the slosh damping coefficient, γ_s, depends on both N_{BO} and N_{GA} for $N_{BO} < 100$. The kind of correlation that fits the data best is $\gamma_s = 0.83\, N_{GA}^{-1/2} (1 + 8.2\, N_{BO}^{-3/5})$, and this correlation reduces to the correct form as $N_{BO} \to \infty$. The γ_s results compare very well to drop tower results,[1] which also show that the preceding correlation is not valid when $N_{BO} < 3$.

Spherical tanks

The N_{BO} range covered in these tests was 43 to 175. Here, N_{BO} is based on the diameter of the liquid free surface, since surface tension forces depend primarily on the free surface size and not on tank size. Liquid filling levels of 15.6, 50.0, and 84.4% of the tank volume were tested, which correspond to an average liquid depth of 25, 50, and 75%, respectively, of the tank diameter. For the same tank and liquid, N_{BO} for 15.6% and 84.4% filling is the same since the free-surface diameters are the same. Nonetheless, the free surface curvature at the 84.4% filling is much greater, because of the 0° contact angle, as shown in Fig. 2. Thus, identical N_{BO}'s have different effects at different fillings.

Typical curves of force amplitude vs excitation are shown in Fig. 3; note the magnitude of the measured forces. The response is reasonably linear, and the largest forces always occur for a half-full tank. When compared to an existing equivalent (mathematical) mechanical model for infinitely large N_{BO}, using the experimental values of γ_s and f_1, the experimental peak forces were found to be about 10% smaller than the model predictions, which is also about the discrepancy for cylindrical tanks when going from $N_{BO} = \infty$ to a moderately small N_{BO}.[4]

The difference in natural and resonant frequency is negligible, because of the small damping, and thus the natural frequency can be determined from the force response curves. The resulting variation of $(2\pi f_1)^2 R_o/g$ with N_{BO} and filling level is displayed in Fig. 4. It can be seen that the data points are consistent with each other since, for equal N_{BO} and fill level, the experimental values are the same, regardless of the tank size or liquid properties used. As indicated previously, N_{BO} has a significantly different effect on f_1 at different liquid levels. At low levels, $(2\pi f_1)^2 R_o/g$ is almost independent of N_{BO}, but at the higher levels, it decreases markedly as N_{BO} decreases. This latter change, moreover, is much more pronounced and in the opposite direction than the frequency change in cylindrical tanks. The experimental results compare very well to a recent theory,[6] which is the solid curve in the figure.

Damping coefficients, computed by the half-bandwidth technique, show that the minimum γ_s occurs for a half-full tank, and that γ_s for the 15.6% filling is about twice that for

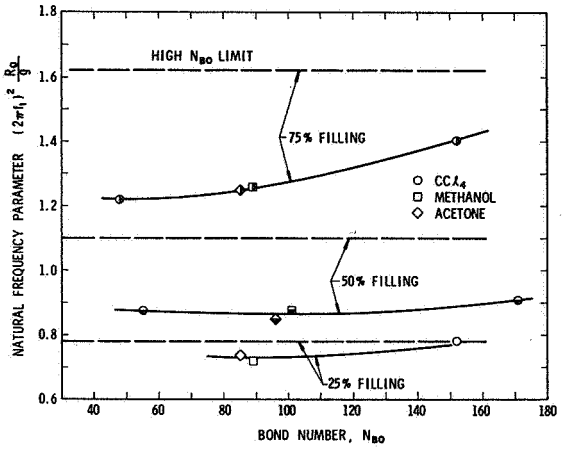

Fig. 6 Variation of natural frequency with Bond number for 1.99/1.0 ellipsoidal tanks.

the 84.4% filling. Similar results hold for large N_{BO} sloshing but, in that case, γ_s for the 15.6 and 84.4% filling are about equal. Thus, once again, the effects of the differences in free surface curvature are evident. Finally, γ_s increases when either N_{GA} or N_{BO} decreases, but an accurate correlation has not yet been obtained.

Ellipsoidal tanks

The N_{BO} range covered in the tests with the oblate ellipsoidal tanks was 48 to 172, based on the free-surface diameter. Liquid filling levels of 25, 50, and 75% of the tank volume were tested; these levels correspond to average liquid depths of 33, 50, and 67% of the minor diameter.

The frequency parameters for the $(2)^{1/2}/1.0$ tank are shown in Fig. 5, and for the 1.99/1.0 tank in Fig. 6. (R_o used in these figures is one-half the major diameter.) The trends shown are the same observed previously in Fig. 4 for spherical tanks, except that here the difference in free-surface curvature between the low and the high filling level is not so great because of the smaller difference in filling levels. There are no existing low-g slosh theories for ellipsoidal tanks of these eccentricities. Damping results are qualitatively similar to those described for spherical tanks.

Conclusions

The method of ultrasmall model simulation of low-gravity propellant sloshing has been shown to give useful data for the prototype N_{BO}'s greater than about ten. The test results show that N_{BO} influences the slosh natural frequency only slightly for cylindrical tanks, but markedly for spherical and ellipsoidal tanks that are over half full. The slosh damping has also been shown to depend upon N_{BO}. Finally, qualitative determinations of the "slosh mass" in an equivalent mechanical model indicate that the amount of liquid participating in the sloshing motion is less than for the corresponding large N_{BO}, hat interface case.

References

[1] Salzman, J. A., Labus, T. L., and Masica, W. J., "An Experimental Investigation of the Frequency and Viscous Damping of Liquids During Weightlessness," TN D-4132, 1967, NASA.

[2] Dodge, F. T., "A Discussion of Laboratory Methods of Simulating Low-Gravity Fluid Mechanics," TR 3, Contract NAS8-20290, 1967, Southwest Research Institute, San Antonio, Texas.

[3] Satterlee, H. M. and Reynolds, W. C., "The Dynamics of the Free Liquid Surface in Cylindrical Containers Under Strong Capillary and Weak Gravity Conditions," TR LG-2, 1964, Dept. of Mechanical Engineering, Stanford Univ.

[4] Dodge, F. T. and Garza, L. R., "Experimental and Theoretical Studies of Liquid Sloshing at Simulated Low Gravity," *Transactions of the ASME, Journal of Applied Mechanics*, Vol. 34, Sept. 1967, pp. 555–562.

[5] Dodge, F. T. and Garza, L. R., "Simulated Low-Gravity Sloshing in Cylindrical Tanks Including Effects of Damping and Small Liquid Depth," *Proceedings of 1968 Heat Transfer and Fluid Mechanics Institute*, Stanford Univ. Press, 1968, pp. 67–76.

[6] Concus, P., Crane, G. E., and Satterlee, H. M., "Small Amplitude Lateral Sloshing in Spheroidal Containers Under Low Gravitational Conditions," Final Report, Contract NAS3-9704, 1969, Lockheed Missiles & Space Corp., Sunnyvale, Calif.

A THEORY FOR LOW-GRAVITY FUEL SLOSHING IN AN ARBITRARY AXISYMMETRIC RIGID TANK

by

WEN-HWA CHU

ASME PAPER 70-APM-EEE, to be published in *Transactions ASME, Journal of Applied Mechanics*

NOTE: The numerical examples in the published paper contain several errors. For that reason, the original examples have been corrected for this report and appear here as Appendix D to the paper.

Introduction

THE behavior and consequences of fuel sloshing in rockets under a high effective gravity were recognized problems which have been quite well understood [1–3].[1] The problem of low-gravity fuel sloshing, characterized by the significant role of interfacial tension, is now a subject of importance for application to coasting rockets or orbital stations.

The equilibrium behavior of fluids at zero and/or low gravity has been studied in references [4–7]. The theoretical determination of an equilibrium interface shape is nonlinear and requires a trial and error procedure for a given contact angle [5, 6].

Satterlee and Reynolds [8] have successfully solved the free sloshing problem in cylindrical containers under low gravity and formulated a variational principle for this purpose. Yeh [9], using a similar approach, solved the free and forced sloshing problem under low-gravity conditions, without force and moment or an equivalent mechanical model. Dodge and Garza [10, 11] performed force measurements under simulated low-gravity conditions and predicted forces and moment for circular cylindrical tanks under lateral (translational) motion. The equivalent spring-mass model was given in [10]. Additional work by Dodge and Garza for other special tanks was given in [12, 13]. A finite-difference approach with application to a hemispherically bottomed cylindrical tank and spheroidal tanks was given by Concus, Crane, and Satterlee in [14, 15].

These investigations indicate a need of a program for a general axisymmetric tank. A preliminary study on liquid sloshing in an arbitrary axisymmetric tank was reported in [16], but it is limited to translational oscillations. It is the object of the present paper to present a seminumerical approach for an arbitrary axisymmetric tank with simplified force and moment calculations and the resultant mechanical model for both pitching and translational oscillations. A general computer program utilizing Winslow method [17] will be completed to obtain sloshing frequencies, slosh mass, and mass-height, for which a brief description is given in Appendix A.

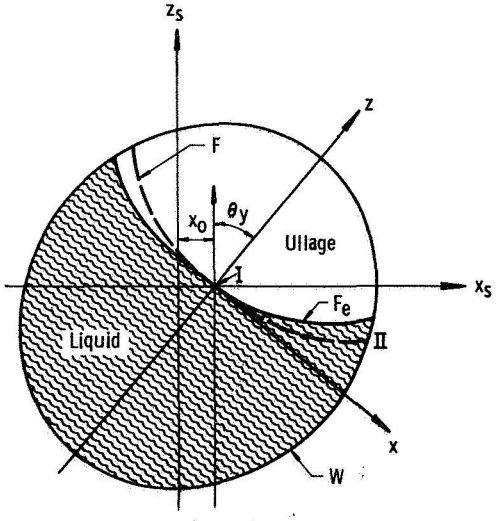

Fig. 1 Some Nomenclatures

[1] Numbers in brackets designate References at end of paper.

Contributed by the Applied Mechanics Division for publication (without presentation) in the JOURNAL OF APPLIED MECHANICS.

Governing Equations

Assuming irrotational incompressible flow, there is a space-fixed velocity potential[2] ϕ satisfying the Laplace equation in both space-fixed and tank-fixed coordinates

$$\nabla_s^2\phi = 0,\ \nabla^2\phi = 0;$$

$$\nabla_s^2 = \frac{\partial^2}{\partial x_s^2} + \frac{\partial^2}{\partial y_s^2} + \frac{\partial^2}{\partial z_s^2},\ \nabla^2 = \frac{\partial^2}{\partial x^2} + \frac{\partial^2}{\partial y^2} + \frac{\partial^2}{\partial z^2} \quad (1)$$

As in thin airfoil theory, the velocity potential can be obtained by imposing boundary conditions on the initial or mean position, but the hydrostatic pressure due to gravity possesses components along both the tank axis z and the lateral axis x, Fig. 1, for pitching oscillations. The linearized Bernoulli's equation states

$$p - p_I + \rho\frac{\partial\phi}{\partial t} + \rho g(z - x\theta_y) = 0 \quad (2)[3]$$

and

$$p - p_{uI} + \rho_u\frac{\partial\phi_u}{\partial t} + \rho_u g(z - x\theta_y) = 0 \quad (3)$$

for the liquid and the ullage, respectively, and p_I, p_{uI} are constants.

Boundary Conditions

The linearized interface kinematic condition states that

$$\frac{\partial h}{\partial t} \cong \frac{\partial\phi}{\partial n} \quad \text{on } F \quad (4)[4]$$

The interface dynamic condition states that

$$-p_- + p_+ = \sigma\kappa = \sigma\kappa_0 + \sigma\kappa' \quad \text{on } F_e \quad (5)$$

For the "mean" interface location f (in general, $p_I = p_I^\circ + p_I'$, p_I°, p_I' being constants),

$$-\sigma\kappa_0 + (\rho - \rho_u)gf - (p_I^\circ - p_{uI}^\circ) = 0 \quad \text{on } F \quad (6)$$

where the curvature of the mean interface, κ_0, is axisymmetric and

$$\kappa_0 = \frac{1}{r}\frac{\partial}{\partial r}\left\{\frac{r\dfrac{\partial f}{\partial r}}{\sqrt{1 + \left(\dfrac{\partial f}{\partial r}\right)^2}}\right\} = \frac{1}{r}\frac{\partial f}{\partial s} + \left(\frac{\partial r}{\partial s}\frac{\partial^2 f}{\partial s^2} - \frac{\partial f}{\partial s}\frac{\partial^2 r}{\partial s^2}\right) \quad (6a)$$

Equation (6) holds for $r = 0$, thus

$$p_I^\circ - p_{uI}^\circ = -2\left(\frac{\partial^2 f}{\partial r^2}\right)_{II}$$

The linearized interface dynamic condition is then

$$-(p_u' - p_{uI}') - \sigma\kappa' + \rho\frac{\partial\phi}{\partial t} - \rho_u\frac{\partial\phi_u}{\partial t} + (\rho - \rho_u)gh\frac{\partial r}{\partial s} - (\rho - \rho_u)gx\theta_y = 0 \quad (7)[5]$$

[2] For example, $\partial\phi/\partial x$ gives velocity component in x-direction with respect to space-fixed coordinates.

[3] Chu, W. H., "Free Surface Condition for Sloshing Resulting From Pitching and Some Corrections," *ARS Journal*, Vol. 30, Nov. 1960, pp. 1093–1094.

[4] A vertical interface description was used but is only successful when $(dF/dR)^{-1}$ does not vanish on the interface.

[5] For sinusoidal oscillations and $m = 1$, $h = 0$, $\phi = \phi_u = 0$, $x = 0$, and $\kappa' = 0$ at point I, thus $p_I' - p_{uI}' = 0$. For other m values, $-p_I' + p_{uI}^\circ = \sigma\kappa_I'$, which will be omitted until needed.

where the perturbation curvature for cos $(m\theta)$ variation is to the first order

$$\kappa' = \frac{\partial^2 h}{\partial \mathbf{s}^2} + \frac{1}{r}\frac{\partial r}{\partial \mathbf{s}}\frac{\partial h}{\partial \mathbf{s}} + \frac{1}{r^2}\frac{\partial^2 h}{\partial \theta^2} + \left[\left(\frac{1}{r}\frac{\partial f}{\partial \mathbf{s}}\right)^2 + \left(\frac{\partial r}{\partial \mathbf{s}}\frac{\partial^2 f}{\partial \mathbf{s}^2} - \frac{\partial f}{\partial \mathbf{s}}\frac{\partial^2 r}{\partial \mathbf{s}^2}\right)^2\right] h \quad (7a)^6$$

m being unity for lateral excitation of a rigid tank. At point I, the origin, $h = 0$, $\phi = 0$, $\kappa' = 0$, and thus $p_I = p_{uI}$. For most analyses, $\rho_u = 0$ was assumed. We shall assume the impulsive pressure in the ullage is negligible, i.e., $\phi_u = 0$. Then, for sinusoidal oscillations with h, ϕ proportional to cos (ωt) and sin (ωt), respectively, equations (7), (7a), and (4) yield

$$-\left\{\frac{1}{R}\frac{\partial}{\partial s}\left(R\frac{\partial H}{\partial s}\right) - \frac{m^2}{R^2}H + GH\right\} + N_{B_e}H\frac{\partial R}{\partial s} + \theta_y N_{B_e} R\cos\theta + \Omega^2\Phi = 0 \quad \text{on } F \quad (7b)^7$$

where

$$G = \left(\frac{1}{R}\frac{\partial F}{\partial s}\right)^2 + \left(\frac{\partial R}{\partial s}\frac{\partial^2 F}{\partial s^2} - \frac{\partial F}{\partial s}\frac{\partial^2 R}{\partial s^2}\right)^2 = \frac{1}{R^2}\frac{{F_R}^2}{(1+{F_R}^2)} + \left[\frac{F_{RR}}{(1+{F_R}^2)^{3/2}}\right]^2 \quad (7c)$$

It is noted that, for lateral oscillations, $m = 1$, solutions are proportional to cos θ.

The boundary condition on the wall is that the relative normal velocity be zero, i.e., with cos $(n, x) = \dfrac{\partial x}{\partial n}$ and cos $(n, z) = \dfrac{\partial z}{\partial n}$,

$$\frac{\partial \phi}{\partial n} = \dot{x}_0\frac{\partial x}{\partial n} \quad (8)$$

and

$$\frac{\partial \phi}{\partial n} = \dot{\theta}_y\left(z\frac{\partial x}{\partial n} - x\frac{\partial z}{\partial n}\right) \quad (9)$$

for translational and pitching oscillations, respectively.

In addition, there is an interface contact point condition which takes the form [8, 9, and 15]

[6] The instantaneous interface can be described by the position vector $\mathbf{r}/a = [R - HF_s]\cos\theta\hat{i} + [R - HF_s]\sin\theta\hat{j} + [F + HR_s]\hat{k}$; $R_s = dR/ds$, $F_s = dR/ds$. The curvatures can then be derived from the fundamental magnitudes [18] neglecting higher-order terms. The linearized total curvature is given by this equation, which was first derived in [15] by a different procedure.

[7] For sinusoidal oscillations, without loss of generality, $\dot{x}_0$, θ_y, ϕ are assumed to be proportional to sin (ωt) while h is proportional to cos (ωt).

Nomenclature

a = reference length, say, maximum radius of tank
$d\mathbf{A}$ = dA/a^2 (a scalar)
dA = $rdrd\theta$
$d\mathbf{S}$ = dS/a^2, nondimensional surface element (a scalar)
dS = 3-D surface element, e.g., $rd\theta d\mathbf{s}$
F = equilibrium (mean) interface of f/a
F_e = instantaneous interface
F_H = horizontal force defined by equation (19)
F_R = (dF/dR), slope of F in the generatrix plane
F_x = x-component of force on tank
f = equilibrium (mean) interface elevation measured along vertical axis
g = gravitational acceleration
H = amplitude of h/a, nondimensional slosh height
h = interface perturbation normal to equilibrium interface
h_0 = reference length, say, depth of liquid at center of tank
M_0, I_0 = rigid mass and moment of inertia of mechanical model
M_F = liquid mass
M_y = pitching moment about y-axis
m_k = kth slosh mass
N_B = Bond number, $\rho a^2 g/\sigma$
n = outer normal
n_0 = n/a, nondimensional normal distance
p = pressure
p_I = equilibrium liquid pressure at origin—a constant
p_u = ullage pressure
p_{uI} = equilibrium ullage pressure at origin—a constant
R = r/a, nondimensional radius
r, θ, z = tank fixed cylindrical coordinates
s = arc length nondimensionalized by a
$\mathbf{s}$ = arc length (a scalar)
t = time
V = volume of liquid divided by a^3
V_L = liquid volume
W = wall wetted by liquid
W_e = instantaneous wetted wall below instantaneous interface, F_e
x_0 = translational amplitude in x_s-direction
x_s, y_s, z_s = space-fixed rectangular coordinates
Γ = γa, nondimensional contact point constant
γ = hysteresis coefficient or contact point constant
$\Delta\rho$ = density difference, $\rho - \rho_u$
δ_{ij} = Kronecker delta
ϵ_1 = sign of $n\cdot\hat{z}$, cos (n, z), or $\partial z/\partial n$
θ_y = amplitude of pitching about y-axis
κ = mean curvature
κ' = perturbation of mean curvature
λ_j = jth eigenvalue $(m = 1)$
λ_{mj} = jth eigenvalue corresponds to mth circumferential mode
ρ = liquid density
ρ_u = density of ullage fluid (vapor or gas)
σ = surface tension
Φ = amplitude of nondimensional velocity potential, $\phi/\omega a^2$
Φ_k = amplitude of nondimensional potential $\phi_k/\omega a^2$
Φ_N = see equation (15)
Φ° = amplitude of nondimensional potential $\phi^\circ/\omega a^2$
ϕ = velocity potential
ϕ_k = velocity potential of the kth natural mode
ϕ' = additional velocity potential due to interface movement
ϕ° = velocity potential of liquid with a frozen interface
ψ = velocity potential of auxiliary eigenfunctions
ψ_j = jth auxiliary characteristic function
Ω^2 = $\rho a^3\omega^2/\sigma$; product of Bond number, $\rho a^2 g/\sigma$, and frequency parameter, $\omega^2 a/g$
ω = frequency of oscillation
ω_k = kth natural frequency

Subscripts

$(\ )_I$ = $(\ )$ at vertex of equilibrium interface (origin)
$(\ )_{II}$ = $(\ )$ at contact point in generatrix plane
$(\ )_{CG}$ = $(\ )$ related to center of gravity
$(\ )_e$ = effective value of $(\ )$
$(\ )_F$ = $(\ )$ on F
$(\ )_m$ = $(\ )$ associated with cos $(m\theta)$ mode
$(\ )_p$ = $(\ )$ related to pitching
$(\ )_T$ = $(\ )$ related to translation
$(\ )_W$ = $(\ )$ on W
$(\ )_u$ = $(\ )$ related to ullage
$(\ )_-$ = $(\ )$ just below interface
$(\ )_+$ = $(\ )$ just above interface

$$\frac{\partial h}{\partial \mathbf{s}} = \gamma h \quad \text{or} \quad \frac{\partial H}{\partial s} = \Gamma H \quad \text{at point II} \tag{10}$$

where γ may be a frequency-dependent constant. However, if the contact angle remains constant, we can show that (see Appendix C[8])

$$\gamma = +\frac{1}{\sin\theta_c}\left\{\left|\frac{z_{rr}}{(1+z_r^2)^{3/2}}\right|_{W,\mathrm{II}} - \cos\theta_c \left|\frac{f_{rr}}{(1+f_r^2)^{3/2}}\right|_{\mathrm{II}}\right\} \tag{10a}$$[9]

$$\Gamma = \gamma a \tag{10b}$$

where

$$z_r = \frac{dz}{dr}, f_r = \frac{df}{dr}, z_{rr} = \frac{d^2z}{dr^2}, f_{rr} = \frac{d^2f}{dr^2}; \quad z \text{ on } W, f \text{ on } F$$

Method of Solution

We shall decompose ϕ into two parts, ϕ' and ϕ°: ϕ° is the velocity potential corresponding to a liquid contained by a rigid mean interface and the tank walls. Therefore, it satisfies the Laplace equation and the nonhomogeneous boundary condition on the contour, equation (8) for translation and equation (9) for pitching on F_e and W_e. It is noted that

$$\phi_T{}^0 = \dot{x}_0 x \tag{11}$$

while $\phi_p{}^\circ$ can be constructed numerically.

ϕ' is the perturbed velocity potential due to sloshing which is governed by the Laplace equation, the zero normal velocity condition at the wall and the resultant interface condition. The first two are satisfied by expansion in normal modes and the last by equations (15) and (16). In this paper, the normal modes are determined by expansion into a set of auxiliary characteristic functions[10] ψ_j, which is orthogonal on the curved interface, and satisfies the Laplace equation and the zero normal velocity wall condition.[11] The interface condition governing normal modes is second order [see equation (7b)] subject to zero H at center and the contact point condition, equation (10a) at wall. The former is satisfied as ψ_j vanishes along tank center line. The interface equation is approximately satisfied by a modified Galerkin method (the strict Galerkin method is given in [19]), which is illustrated in Appendix B. In this method, the contact point condition was imposed on the whole series, not term by term. The numerical results shown later substantiate the method used.

The force and moment are obtained by integration of pressure, not only on the wall, but also on the interface since the direct surface tension force and moment on the tank is equivalent to those on the interface due to pressure, assuming the interface inertia is negligible, as well as the interface mass. To put results in the mechanical model form, the divergence theorem has been most useful (with some manipulations).

Analytical Results

Free Oscillations. For free oscillations, the natural mode ϕ_k is expanded into a truncated series of the auxiliary eigenfunctions, i.e.,

$$\Phi_k = \frac{\phi_k}{\omega a^2} = \sum_{j=1}^{j_{mx}} c_{kj}\psi_{m_j}\cos(m\theta),\ \psi_j = \psi_{m_j}\cos(m\theta) \tag{12a, b}$$

$$H_k = \frac{h_k}{a} = -\sum_{j=1}^{J_{mx}} c_{kj}\psi_{m_j}\cos(m\theta) \tag{12c}$$

c_{kj} is the kth eigenvector of the following matrix equation obtained by a modified Galerkin method (Appendix B) from integrating the nondomensional equation (7b) with $\theta_y = 0$ and weighting function $\psi_{m_i} dS/\alpha_{m_i}{}^2$:

$$\left\{-\Gamma[\nu_{m_{ij}}] + [\gamma_{m_{ij}}] + m^2[\epsilon_{m_{ij}}] + \frac{\Delta\rho}{\rho}N_B[\beta_{m_{ij}}] - \Omega^2[\Delta_{m_{ij}}]\right\}\{c_j\} = 0;\ i, j = 1 \text{ to } J_{mx} \tag{13}$$

where

$$\beta_{m_{ij}} = \frac{\lambda_{m_{ij}}}{\alpha_{m_i}{}^2}\int_F \frac{\psi_{m_i}\psi_{m_j}\epsilon_1}{\sqrt{1+F_R{}^2}}\,dS,\ \epsilon_1 = \mathrm{sgn}\left(\frac{\partial R}{\partial s}\right) \tag{13a}$$[12]

$$\epsilon_{m_{ij}} = \frac{\lambda_{m_j}}{\alpha^2{}_{m_i}}\int_F \frac{1}{R^2}\psi_{m_i}\psi_{m_j}dS \tag{13b}$$

$$\nu_{m_i} = \frac{2\pi\lambda_{m_{ij}}}{\alpha_{m_i}{}^2}[R\psi_{m_i}\psi_{m_j}] \tag{13c}$$

$$\gamma_{m_{ij}} = \frac{\lambda_{m_j}}{\alpha_{m_i}{}^2}\left\{\int_F [1+F_R{}^2]^{-1}\frac{d\psi_{m_i}}{dR}\frac{d\psi_{m_j}}{dR}\,dS - \int_F G\psi_{m_i}\psi_{m_j}\,dS\right\} \tag{13d}$$

$$\Delta_{m_{ij}} = \frac{1}{\alpha_{m_i}{}^2}\int_F \psi_{m_i}\psi_{m_j}\,dS = \delta_{ij} \tag{13e}$$

$$\alpha_{m_i}{}^2 = \int_F \psi_{m_i}{}^2\,dS \tag{13f}$$

and $m = 1$ for lateral excitation of a rigid tank.

Forced Oscillations. Let

$$\phi' = -\omega a^2\sum_{k=1}^{K_{mx}} d_k\Phi_k;\ d_k = \frac{\bar{d}_k\Omega^2}{\Omega_k{}^2 - \Omega^2};\ \Phi_k = \sum_{j=1}^{J_{mx}} c_{kj}\psi_j \tag{14a, b, c}$$

in order to satisfy the interface condition that

$$\sum_{k=1}^{K_{mx}} d_k(\Omega_k{}^2 - \Omega^2)\Phi_k = -\Omega^2\Phi^\circ + \epsilon_2 N_B\frac{\Delta\rho}{\rho}\frac{x}{a}\theta_y \equiv \Phi_N\Omega^2 \tag{15}$$

$\epsilon_2 = 0$ for translational oscillation, $\epsilon_2 = 1$ for pitching oscillation. We have by the Galerkin procedure [19, equation (115.5), p. 435]

$$\sum_{k=1}^{K_{mx}} \bar{d}_k\int_F \Phi_k(-H_l)dS = \int_F \Phi_N(-H_l)dS,\ l = 1 \text{ to } K_{mx} \tag{16}$$

A weighting function of H_l was used taking advantage of the biorthogonal relation, equation (17). This assures the first K_{mx} components of the error as series in ϕ_k be zero. $\bar{d}_k$ can be solved from equation (16) by matrix inversion. There is no need of storing information of ψ_j inside the fluid domain as only the force and moment are of interest. It is noted in the limit [8 and 9]

$$\int_F \Phi_k(-H_l)dS = \delta_{kl}\int_F \Phi_k(-H_k)dS \tag{17}$$[13]

[8] Appendix is not in order of mention.

[9] An equivalent form was first derived in reference [15].

[10] For direct application of the Winslow method [17], we impose the simpler normal derivation condition, $\partial\psi_j/\partial n_0 = \lambda\psi_j$, on F and used the well-known influence coefficient technique to determine the eigenvector ψ_j on the intersurface, the eigenvalue λ_j.

[11] Strictly speaking, the boundary conditions are imposed in Winslow method, while the solution not proven to satisfy these conditions is correct on physical grounds (see Appendix A).

[12] The orthogonality property of ψ_j, thus, ψ_{m_j}, can be easily proved [16] as in the high-G case. $\cos^2(m\theta)$ in the integrand are uniformly omitted as they contribute the same factor, 1/2.

[13] This is referred to as biorthogonal relation.

then,

$$\bar{d}_l = \frac{\int_F \Phi_N(-H_l)dS}{\int_F \Phi_l(-H_l)dS} \tag{18}$$

which was utilized in proving that a unique spring-mass system exists for both pitching and translation.

Force and Moment. The force and moment exerted by a spring-mass system, Fig. 2, without damping were written in the following form [20] and remain valid if contributions due to direct surface tension are included

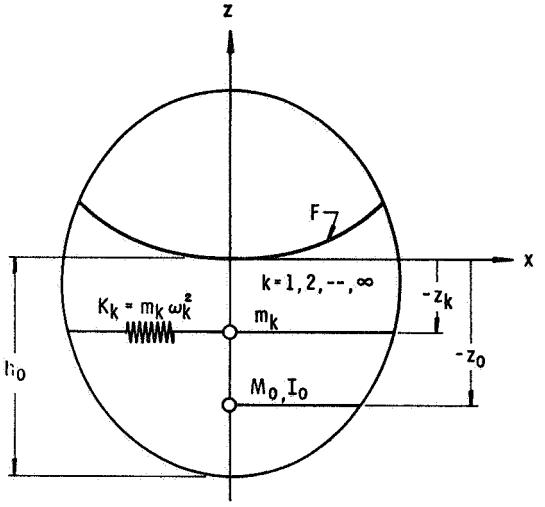

Fig. 2 Equivalent mechanical model

$$F_H = F_x - M_F g\theta_y \tag{19}$$

$$F_{H_T} = x_0\omega^2 M_F \left\{1 + \sum_{k=1}^{\infty} \frac{m_k}{M_F} \frac{1}{\left(\frac{\omega_k^2}{\omega^2} - 1\right)}\right\} \tag{20}$$

$$M_{y_T} = x_0\omega^2 M_F h_0 \left\{\frac{z_{CG}}{h_0} + \sum_{k=1}^{\infty} \frac{m_k}{M_F}\left(\frac{z_k}{h_0} + \frac{g}{h_0\omega^2}\right) \frac{1}{\left(\frac{\omega_k^2}{\omega^2} - 1\right)}\right\} \tag{21}$$

$$F_{H_p} = \theta_y\omega^2 M_F h_0 \left\{\frac{z_{CG}}{h_0} + \sum_{k=1}^{\infty} \frac{m_k}{M_F}\left(\frac{z_k}{h_0} + \frac{g}{h_0\omega^2}\right) \frac{1}{\left(\frac{\omega_k^2}{\omega^2} - 1\right)}\right\} \tag{22}$$

$$M_{y_p} = \theta_y\omega^2 M_F h_0^2 \left\{\frac{I_F}{M_F h_0^2} + \sum_{k=1}^{\infty} \frac{m_k}{M_F}\left(\frac{z_k}{h_0} + \frac{g}{\omega^2 h_0}\right)^2 \frac{1}{\left(\frac{\omega_k^2}{\omega^2} - 1\right)}\right\} + \theta_y g M_F h_0 \left(\frac{z_{CG}}{h_0}\right) \tag{23}$$

with rigid mass m_0, its location z_0, and moment of inertia I_0 given by

$$\frac{m_0}{M_F} = 1 - \sum_{k=1}^{\infty} \frac{m_k}{M_F} \tag{24}$$

$$\frac{z_0}{h_0} = \frac{1}{\frac{m_0}{M_F}}\left[\frac{z_{CG}}{h_0} - \sum_{k=1}^{\infty} \frac{z_k}{h_0}\frac{m_k}{M_F}\right] \tag{25}$$

$$\frac{I_0}{M_F h_0^2} = \frac{I_F}{M_F h_0^2} - \left(\frac{m_0}{M_F}\frac{z_0^2}{h_0^2} + \sum_{k=1}^{\infty} \frac{m_k}{M_F}\frac{z_k^2}{h_0^2}\right) \tag{26}$$

The force due to liquid pressure and direct surface tension is

$$F_x = \int_{W_e+F_e} p\,\frac{\partial x}{\partial n}\,dS \tag{27}$$[14]

and the moment due to liquid pressure and direct surface tension is

$$M_y = \int_{W_e+F_e} p\left(z\,\frac{\partial x}{\partial n} - x\,\frac{\partial z}{\partial n}\right) dS \tag{28}$$

it can be shown that

$$\frac{m_k}{M_F} = \bar{d}_{kT} f_k' \frac{1}{V} \tag{29}$$

where

$$f_k' = \sum_{j=1}^{\infty} c_{kj} \int_F \lambda_j \psi_j \frac{x}{a}\,d\mathbf{S} \tag{29a}$$

$$\bar{d}_{kT} = \frac{1}{\beta_k^2}\int_{W+F} \Phi_k \frac{\partial x}{\partial n}\,d\mathbf{S} \cong \frac{1}{\beta_k^2}\sum_{j=1}^{J_{mx}} c_{kj}\lambda_j \int_F \frac{x}{a}\psi_j\,d\mathbf{S} \tag{29b}$$[15]

$$V = V_L/\rho a^3,\ \beta_k^2 = \int_F \Phi_k(-H_k)d\mathbf{A} \tag{29c, d}$$

and

$$\frac{z_k}{a} = \frac{1}{\frac{m_k}{M_F}}\left(\frac{l_k'}{V}\right) \tag{30}$$

where

$$l_k' = \bar{d}_{kT}\sum_{j=1}^{\infty} c_{kj}\mu_j \tag{30a}$$

$$\mu_j = \int_{F+W} \psi_j \left(\frac{z}{a}\frac{\partial x}{\partial n} - \frac{x}{a}\frac{\partial z}{\partial n}\right) d\mathbf{S} \tag{30b}$$

and that

$$I_F = M_F a^2 I_F^*,\ I_F^* \cong \frac{1}{V}\int_{W+F} \Phi_p{}^{\circ} \left(\frac{z}{a}\frac{\partial r}{\partial n} - \frac{x}{a}\frac{\partial z}{\partial n}\right) d\mathbf{S} \tag{31a, b}$$

In deriving the mechanical model, ρ_u has been set to zero. A simple modification can be made for small ullage density by using

$$N_{B_e} = \frac{\Delta\rho}{\rho} N_B$$

the effective Bond number instead of the Bond number based on the density of the liquid, provided that the dynamic pressure due

[14] It is important to note that great simplification in results, when reduced to the mechanical model for both translation and pitching, is achieved by consideration of balance of forces acting on the thin interface as a free body. The force and moment on the tank due to direct surface tension must be equal to those acting on the interface by liquid pressure. These were not included in reference [15].

[15] For finite J_{mx}, it was found that $\bar{d}_{kT}$, determined by matrix inversion of equation (16) without using biorthogonal relation, yields results in better agreement with Dodge's theory [12] than equation (29b) which is correct in the limit.

to ullage motion is negligible.

It is noted that to prove the mechanical model for pitching motion frequent application of divergence theorem combined with differential properties of the auxiliary characteristic functions and the coordinate functions x and z were used. For brevity, the details are not included in this paper.

Numerical Examples. The present computer program has been checked out for several examples in Appendix III. These include cylindrical tanks, spherical tanks, and spheroidal tanks. Good agreement of first spring-mass with known theory or experiments was obtained with as few as 11 or 12 interface net points and the first seven auxiliary characteristic functions. Finer nets may yield higher accuracies, especially for the higher modes.

Machine Time. For a 12 × 18 mesh and a 12 × 12 mesh, the CDC-6600 central process time is a little over 2 min, while for the 23 × 34 mesh it is about 21 min. Most of the computing time was expended for the generation of influence coefficients, each of which is a Neumann problem. However, the influence coefficient method may be more convenient than the inversion of a large matrix, if not faster. No computer running time was reported in references [14 and 15], which finds natural modes by finite-differences and (partial) matrix inversion.

Conclusion

It seems that the present method yielded a practical way of computing the fundamental natural frequency, the first slosh mass, and its location. Higher masses and locations are usually not needed for design purposes and can be obtained by using finer meshes and longer machine time. A computer program utilizing triangular meshes and Winslow method [17] has been successfully employed and is expected to be completed in the near future for the titled problem. However, the present logical diagram may be limited to a convex axisymmetric tank for good accuracy.

Acknowledgments

The author would like to take this opportunity to thank D. R. Saathoff, A. F. Mueller, and R. Gonzales for writing the computer programs, and Dr. Franklin T. Dodge for his helpful discussions. The present research is supported by NASA Contract NAS8-20290, George C. Marshall Space Flight Center.

References

1 Abramson, H. N., ed., "The Dynamic Behavior of Liquids in Moving Containers," NASA Office of Scientific and Technical Information SP-106, Washington, 1966.

2 Abramson, H. N., "Dynamic Behavior of Liquids in Moving Containers," *Applied Mechanics Reviews*, Vol. 16, No. 7, July 1963, pp. 501–506.

3 Cooper, R. M., "Dynamics of Liquids in Moving Containers," *ARS Journal*, Vol. 30, Aug. 1960, p. 725.

4 Neu, J. T., and Good, R. J., "Equilibrium Behavior of Fluids in Containers at Zero-Gravity," *AIAA Journal*, Vol. 1, No. 4, Apr. 1963, pp. 814–819.

5 Satterlee, H. M., and Chin, J. H., "Meniscus Shape Under Reduced-Gravity Conditions," Symposium on Fluid Mechanics and Heat Transfer Under Low Gravitational Conditions, June 1965.

6 Hastings, L. J., and Rutherford, R., III, "Low Gravity Liquid-Vapor Interface Shapes in Axisymmetric Containers and a Computer Solution," NASA TM X-53790, Oct. 1968.

7 Petrash, D. A., and Otto, E. W., "Studies of the Liquid Vapor Interface Configuration in Weightlessness," ARS Space Power System Conference, Santa Monica, Calif., Paper No. 2514-62, 1962.

8 Satterlee, H. M., and Reynolds, W. C., "The Dynamics of the Free Liquid Surface in Cylindridal Containers Under Strong Capillary and Weak Gravity Conditions," TR LG-2, Department of Mechanical Engineering, Stanford University, May 1, 1964.

9 Yeh, G. C. K., "Free and Forced Oscillations of a Liquid in an Axisymmetric Tank at Low-Gravity Environments," JOURNAL OF APPLIED MECHANICS, Vol. 34, No. 1, TRANS. ASME, Vol. 89, Series E, Mar. 1967, pp. 23–28.

10 Dodge, F. T., and Garza, L. R., "Experimental and Theoretical Studies of Liquid Sloshing at Simulated Low Gravities," Technical Report No. 2, Contract No. NAS8-20290, Control No. DCN 1-6-75-00010, SwRI Project 02-1846, Southwest Research Institute, Oct. 1966; see also JOURNAL OF APPLIED MECHANICS, Vol. 34, No. 3, TRANS. ASME, Vol. 89, Series E, Sept. 1967, pp. 555–562.

11 Dodge, F. T., and Garza, L. R., "Simulated Low-Gravity Sloshing in a Cylindrical Tank Including Effects of Damping and Small Liquid Depth," *Proceedings, 1968 Heat Transfer and Fluid Mechanics Institute*, Stanford University Press, 1968, pp. 67–69.

12 Dodge, F. T., and Garza, L. R., "Simulated Low-Gravity Sloshing in Spherical Tanks and Cylindrical Tanks With Inverted Ellipsoidal Bottoms," Technical Report No. 6, Contract NAS8-20290, Control No. DCN 1-6-75-00010, SwRI Project No. 02-1846, Southwest Research Institute, Feb. 1968.

13 Dodge, F. T., and Garza, L. R., "Slosh Force, Natural Frequency, and Damping of Low-Gravity Sloshing in Oblated Ellipsoidal Tanks," Technical Report No. 7, Contract No. NAS8-20290, Control No. DCN 8-75-00043(IF), SwRI Project No. 02-1846, Southwest Research Institute, Feb. 1969.

14 Concus, P., Crane, G. E., and Satterlee, H. M., "Low Gravity Lateral Sloshing in Hemispherically Bottomed Cylindrical Tanks," *Proceedings, 1968 Heat Transfer and Fluid Mechanics Institute*, Stanford University Press, 1968, pp. 80–97.

15 Concus, P., Crane, G. E., and Satterlee, H. M., "Small Amplitude Lateral Sloshing in Spheroidal Containers Under Low Gravity Conditions," NASA CR-72500, LMSC-A944673, Lockheed Missiles and Space Co., Sunnyvale, Calif., February 4, 1969.

16 Chu, W. H., "Low Gravity Liquid Sloshing in an Arbitrary Asixymmetric Tank Performing Translational Oscillations," Technical Report No. 4, Contact No. NAS8-20290, Control No. DCN 1-6-75 00010, SwRI Project No. 02-1846, Southwest Research Institute, Mar. 1967.

17 Winslow, A. M., "Numerical Solutions of the Quasilinear Poison Equations in a Nonuniform Triangular Mesh," *Journal of Computational Physics*, Vol. 1, No. 2, Nov. 1966, pp. 149–172.

18 Wang, C. T., *Applied Elasticity*, McGraw-Hill, New York, 1953.

19 Sokolnikoff, I. S., *Mathematical Theory of Elasticity*, 2nd ed. McGraw-Hill, New York, 1956.

20 Abramson, H. N., Chu, W. H., and Ransleben, G. E., Jr., "Representation of Fuel Sloshing in Cylindrical Tanks by an Equivalent Mechanical Model," *ARS Journal*, Dec. 1961, pp. 1697–1705.

APPENDIX A

Brief Description of a Computer Program

The following steps of a computer program are briefly described.

Construction of a Triangular Mesh. The triangular mesh is generated as described in reference [17] except that a simple parallelogram is used as the logical diagram, Fig. 3. For a cylindrical tank at Bond number 100, the physical diagram is shown in Fig.

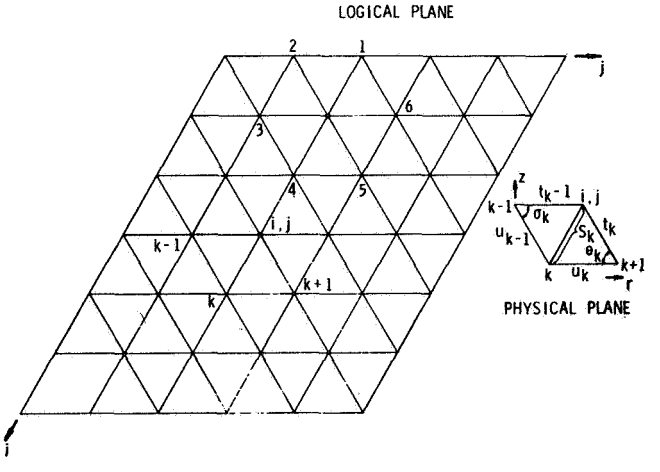

Fig. 3 Simple logical diagram for triangular mesh

4(*a*). For a spheroidal tank ($e = 0.5$) at Bond number 5, a triangular mesh is shown in Fig. 4(*b*). The lengths of the edge of the parallelogram can be adjusted for each individual case to yield desired triangular meshes. A continuous wall needs to be broken into two parts for the logical diagram. This only affects the local distribution of the triangular mesh and has shown to yield good results for a spheroidal tank, as well as a cylindrical tank.

Construction of Auxiliary Characteristic Functions. The characteristic functions ψ satisfy

$$\nabla^2\psi = 0 \tag{32}$$

$$\frac{\partial\psi}{\partial n_0} = 0 \quad \text{on } W \tag{33}$$

$$\frac{\partial\psi}{\partial n_0} = \lambda\psi \quad \text{on } F \tag{34}$$

ψ can be solved numerically with the constructed triangular mesh by Winslow method [17]. Contact point is treated as one of the mesh points, as are the other boundary points.[16] Hence, $\partial\psi/\partial n$ may be discontinuous at the contact point. Zero contact angle cannot be constructed graphically but results of decrease mesh size give closer and closer approximations to the interface and would probably lead to the correct limiting value.

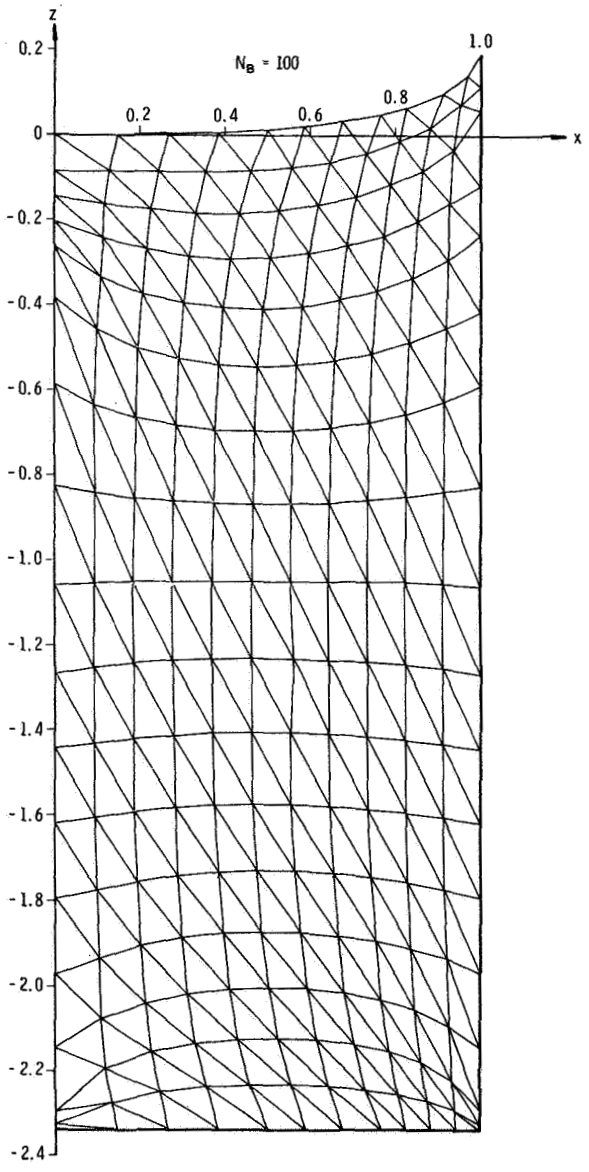

Fig. 4(a) Physical diagram of triangular mesh—cylindrical tank

For an interior joint, ij, [$\psi = \psi_{ij}$, $\psi_k = \psi_k(i, j)$, $r_k = r_k(i, j)$, $r = r_{ij}$]

$$\sum_{k=1}^{6} \omega_k(\psi_k - \psi) - \frac{m^2}{r_{ij}} A_{ij}\psi = 0 \tag{35}$$

where

A_{ij} = area of the ijth dodecagon [17] inside the fluid domain
r_{ij} = radius of the ijth point

$$\omega_k = \tfrac{1}{2}(\lambda_k \bar{r}_k \cot\theta_k + \lambda_{k-1}\bar{r}_{k-1}\cot\sigma_k) \quad k = 1 \text{ to } 6 \tag{35a}[17]$$

$$\bar{r}_k = \tfrac{1}{3}(r_{ij} + r_k + r_{k+1}) \quad \lambda_k = 1 \tag{35b, c}$$

θ_k, σ_k, Fig. 3, can be expressed in terms of t_k, u_{k+1}, t_{k-1}, u_{k-1}, and s_k.

For interface point,

$$\sum_{k=1}^{6} \omega_k(\psi_k - \psi) - \frac{m^2}{r_{ij}} A_{ij}\psi + \left(\frac{\partial\psi}{\partial n}\right)_{1,j}\left[\frac{1}{2}s_3 + \frac{1}{2}s_6\right] r_{ij} = 0 \tag{36}$$

where

$$\lambda_6 = \lambda_1 = \lambda_2 = 0, \quad \lambda_3 = \lambda_4 = \lambda_5 = 1$$

To solve for the eigenfunctions on the interface, we use the influence coefficient method in which $(\partial\psi/\partial n)_{1,i} = 0$ except $(\partial\psi/\partial n)_{1,j} = 1$ for the jth column of the influence matrix. A standard eigenvalue problem involving only the interface points, excluding $\psi_{1,1}$ at $r = 0$, is needed to obtain the eigenvalues λ_j and eigenvectors ψ_j. Knowing the jth eigenvector on the interface, the corresponding value of ψ_j on the wall can be easily solved numerically again by the method of overrelaxation.

For ijth point on the tank wall

$$\sum_{k=1}^{6} \omega_k(\psi_k - \psi) - \frac{m^2}{r_{ij}} A_{ij}\psi = 0 \tag{37}$$

$\lambda_3 = \lambda_4 = \lambda_5 = 0$ and $\lambda_1 = \lambda_2 = \lambda_6 = 1$ on the bottom wall

$\lambda_4 = \lambda_5 = \lambda_6 = 0$ and $\lambda_1 = \lambda_2 = \lambda_3 = 1$ on the side wall

On center line, $r = 0$,

$$\psi = 0 \text{ for } m \geq 1$$
$$\frac{\partial\psi}{\partial r} = 0 \text{ for } m = 0 \tag{38}$$

$$\lambda_1 = \lambda_2 = \lambda_3 = 0 \text{ and } \lambda_4 = \lambda_5 = \lambda_6 = 1$$

At contact point $i = 1, j = j_{mx}$.

$$\sum_{k=1}^{6} \omega_k(\psi_k - \psi) - \frac{m^2}{r_{ij}} A_{ij}\psi + \left(\frac{\partial\psi}{\partial n}\right)_{1,j_{mx}}\left(\frac{1}{2}s_3\right) r_{ij} = 0 \tag{39}$$

$$\lambda_3 = 1, \lambda_1 = \lambda_2 = \lambda_4 = \lambda_5 = \lambda_6 = 0$$

Calculation of Interface Shape. A program based on the theory of reference [6] was written to generate the interface shape with desired net points for a given empty fraction or central depth and a

[16] This represents conservation of mass in the triangle containing contact point. Experience shows that the contact point condition should not be imposed on ψ_j.

[17] Note: $(\lambda_{j-1/2})$ reference [17] $= \lambda_{j-1}$, $(\lambda_{j+1/2})$ reference [17] $= \lambda_j$.

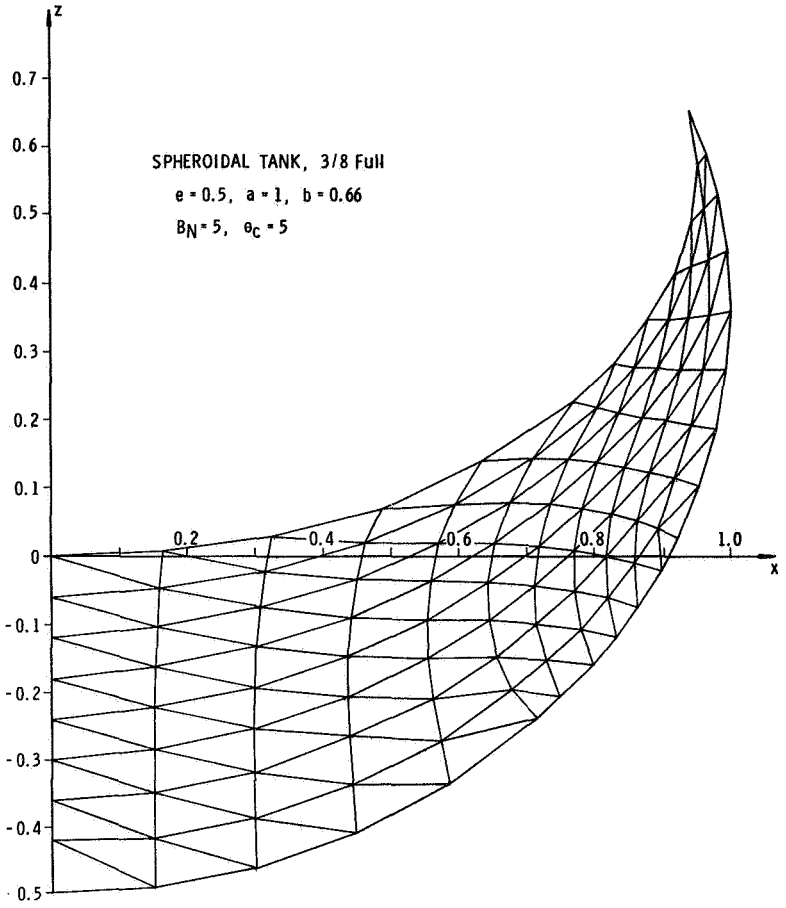

Fig. 4(b) Triangular mesh for spheroidal tank at low gravity

given contact angle. This program also calculates contact point constant Γ but limits the contact angle to possibly 2 deg or greater.

Calculation of Natural Frequencies, Slosh Masses, and Their Location

The remaining steps are relatively routine and, therefore, will not be described. It is, however, remarked that trapezoidal rule and midpoint rules were employed conveniently in evaluating the integrals. For some quantities, quadratic fittings were made, such as dF/dR, before entering the quadrature formulas.

APPENDIX B

A Modified Galerkin Method

In the Galerkin method, it is generally assumed [19] that each of the coordinate functions of a complete set satisfies the same boundary conditions as the exact solution. This condition seems to be a sufficient condition rather than a necessary condition since the series expansion as a whole may satisfy the prescribed conditions, not necessarily term by term. Since the solution, if continuous, can be expanded into a convergent series containing the complete set, the failure of the error minimization process, if it occurs, must lie in the insufficient differentiability of the series. Therefore, the present method as applied to a second-order ordinary differential equation performs integration by part, then imposes the remaining boundary condition[18] as illustrated by the following example.

Let y be governed by the simple equation

$$\frac{d^2y}{dx^2} + \lambda^2 y = 0; \qquad \lambda \neq \frac{2m-1}{2}\pi \tag{40}$$

subject to

$$y = 0 \qquad \text{at } x = 0 \tag{41}$$

$$\frac{dy}{dx} = \Gamma_1 \qquad \text{at } x = 1 \tag{42}$$

We shall select a complete set in (0, 1) which satisfies $y = 0$ at $x = 0$ but $y \neq 0$ at $x = 1$. To be specific, we express

$$y = \sum_{m=1}^{\infty} C_m \sin(\lambda_m x) \tag{43}$$

where

$$\lambda_m = \frac{2m-1}{2}\pi$$

Then, the modified Galerkin procedure minimizes the error of the differential equation as follows:

$$0 = \int_0^1 \sin(\lambda_n x)\left[\frac{d^2y}{dx^2} + \lambda^2 y\right] dx$$

$$= \left[\sin(\lambda_n x)\frac{dy}{dx}\right]_0^1 - \int_0^1 \lambda_n \frac{dy}{dx}\cos(\lambda_n x)dx$$

$$+ \int_0^1 \lambda^2 y \sin(\lambda_n x)dx = (-1)^{n-1}\Gamma_1$$

$$- \int_0^1 \lambda_n \lambda_m \sum_{m=1}^{\infty} C_m \cos(\lambda_n x)\cos(\lambda_m x)dx$$

[18] This may be a new technique to satisfy the boundary condition or conditions. However, a general proof and extension remain to be done.

$$+ \int_0^1 \lambda^2 \sum_{m=1}^{\infty} C_m \sin(\lambda_n x) \sin(\lambda_m x) dx$$

$$= (-1)^{n-1}\Gamma_1 - \left(\frac{\lambda_n^2}{2} - \frac{\lambda^2}{2}\right) C_n, \qquad n = 1, 2, \ldots, \infty \quad (44)$$

Thus

$$C_n = \frac{2\Gamma_1(-1)^{n-1}}{(\lambda_n^2 - \lambda^2)} \quad (45)$$

The exact solution of the problem is

$$y = \frac{\Gamma_1}{\lambda \cos \lambda} \sin(\lambda x) = \sum_{n=1}^{\infty} C_n' \sin(\lambda_n x) \quad (46)$$

It is easy to show that the Fourier coefficient C_n' of the exact solution is equal to C_n; thus the modified Galerkin method yields the exact solution in the limit.

The rate of convergence of the foregoing example ($\Gamma_1 \neq 0$) is only $1/n^2$ near the end, $x = 1$. This could be expected as dy/dx is zero term by term while with infinite terms converge to Γ_1 as a whole when $x \to 1$. Equation (13) in the text is analogously derived; however, the rate of convergence might be better as illustrated by results in Appendix III. It should be pointed out that at the high Bond numbers, each auxiliary characteristic function is a normal mode and, as Bond number decreases, more characteristic functions are required to represent each mode. Only by actual computation is one to find out how many of them are sufficient for engineering purposes.

APPENDIX C

Constant Contact Angle Condition

For small perturbed motions at the instantaneous contact point, Part 2, Fig. 5.

$$\theta_2 = \theta_1 + \beta \quad (47)$$

$$= \theta_0 + \left(\frac{\partial \theta_0}{\partial s}\right)_{II} dS_F + \left(\frac{\partial h}{\partial s}\right)_{II} \quad (48)$$

With $\tan \theta_0 = \frac{df}{dr}$, $\frac{dr}{ds} = \frac{\epsilon_1}{\sqrt{1 + f_r^2}}$, $\epsilon_1 = \operatorname{sgn}\left(\frac{dr}{df}\right)$, one has

$$\left(\frac{\partial \theta_0}{\partial s}\right)_{II} = \sec^2 \theta_0 \left(\frac{d^2 f}{dr^2} \frac{\epsilon_1}{\sqrt{1 + f_r^2}}\right)_{II} = \left[\frac{f_{rr}\epsilon_1}{(1 + f_r^2)^{3/2}}\right]_{II} \quad (49)$$

Similarly, at the instantaneous contact point 2,

$$\theta_{W_2} = \theta_{WII} + \left(\frac{\partial \theta_W}{\partial s_W}\right)_{II} ds_W \quad (50)$$

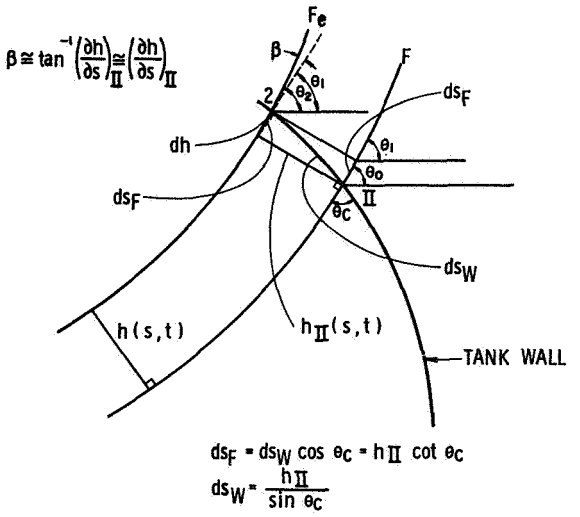

$$ds_F = ds_W \cos \theta_C = h_{II} \cot \theta_C$$

$$ds_W = \frac{h_{II}}{\sin \theta_C}$$

Fig. 5 Geometry for contact point condition

$$= \theta_{WII} + \left[\frac{z_{rr}\epsilon_2}{(1 + z_r^2)^{3/2}}\right]_{W,II} ds_W \quad (51)$$

where

$$\epsilon_2 = \operatorname{sgn}\left(\frac{dz}{dr}\right)$$

We shall assume constant contact angle independent of time t, i.e.,

$$\theta_c = \theta_{WII} - \theta_0 = \theta_{W_2} - \theta_2 = \text{const} \quad (52)$$

then, with $dS_W = \frac{h}{\sin \theta_c}$, $dS_F = dS_W \cos \theta_c$, Fig. 6.

$$\frac{f_{rr}\epsilon_1}{[1 + f_r^2]^{3/2}} \cos \theta_c \frac{h}{\sin \theta_c} + \frac{\partial h}{\partial s} - \frac{z_{RR}\epsilon_2}{[1 + z_R^2]^{3/2}} \frac{h}{\sin \theta_c} = 0 \quad \text{at II} \quad (53)$$

i.e.,

$$\frac{\partial h}{\partial s} = \gamma h \quad (54)$$

where

$$\gamma = \frac{1}{\sin \theta_c}\left[\frac{z_{rr}\epsilon_2}{(1 + z_r^2)^{3/2}} - \cos \theta_c \frac{f_{rr}\epsilon_1}{(1 + f_r^2)^{3/2}}\right]_{II} \quad (55)$$

For a convex tank with convex interface

$$\gamma = \frac{1}{\sin \theta_c}\left\{\left|\frac{z_{rr}}{(1 + z_r^2)^{3/2}}\right|_{W,II} - \cos \theta_c \left|\frac{f}{(1 + f_r^2)^{3/2}}\right|_{II}\right\} \quad (56)$$

APPENDIX D. NUMERICAL EXAMPLES

A. Flat Interface with High Bond Number in a Cylindrical Tank $N_B = 1000$, $\frac{h_o}{a} = 2.34$, $a = 0.68$ with $\Gamma = 0$, a 12×18 mesh yielded $\frac{\omega_1^2 a}{g} = 1.85$ compared with 1.847 from exact theory (Ref. 1 of Appendix B).

$\frac{m_1}{m_F} = 0.193$ compared with 0.194 from high-G theory (Ref. 19 of Appendix B).

$z_1 = -0.729$ in. compared with -0.724 in. from high-G theory (Ref. 19 of Appendix B).

B. Flat Interface with Low Bond Number in a Cylindrical Tank $N_B = 10$, $\frac{h_o}{a} = 2.34$, $a = 0.68$ with $\Gamma = 0$, 12×18 mesh yielded $\frac{\omega_1^2 a}{g} = 2.15$ compared with 2.46 from exact theory. A finer mesh is required for better agreement.

C. Curved Interface with Low Bond Number $N_B = 100$, $\frac{h_o}{a} = 2.34$, $a = 0.68$, $\theta_c = 2°$ yielded $\frac{\omega_1^2 a}{g} = 1.860$, $\frac{m_1}{\rho a^3} = 0.442$, $z_1 \cong -0.724$ in. compared with theoretical value of $\frac{\omega_1^2 a}{g} = 1.777$, $\frac{m_1}{\rho a^3} = 0.438$, $z_1 \cong -0.73$ in. (Ref. 12 of Appendix B). It is noted that experimental value of $\frac{\omega_1^2 a}{g}$ for $\theta_c = 0°$ is around 1.78 to 1.80. Finer net may lead to better approximation.

D. Spherical Tank with Flat Interface $N_B = 1000$, $\frac{h_o}{a} = 1$, $a = 1$ with $\Gamma = 0$, 11×11 mesh yielded $\frac{\omega_1^2 a}{g} = 1.54$ compared with high-G sloshing value of $\frac{\omega_1^2 a}{g} = 1.54$.

E. Spherical Tank with "Folding" Interface $N_B = 10$, $\frac{h_o}{a} \cong 1.14$*, $a = 1$, $\theta_c = 4.96°$ ($\Gamma = -65.788$), 12×12 mesh yield $\frac{\omega_1^2 a}{g} = 1.469$, $\frac{m_1}{\rho a^3} = 0.604$, $z_1 = -0.742$ in. compared with Lockheed result (Ref. 16 of Appendix B) of $\frac{\omega_1^2 a}{g} = 1.507$ (for $\theta_c = 5°$). The first slosh mass is much larger than that of Lockheed, probably due to the inclusion of force directly attributed to surface tension in the present theory which yielded confirmed results for cylindrical tanks (Case 3). The value of z_1 would be the location of the center of the sphere if the contribution due to direct surface tension [i.e., the integral over F in Eq. (30b)] is neglected.

F. Spheroidal Tank with Folding Interface Ellipticity $e = 0.5$, major axis $a = 1$, minor axis $b = 0.866$, $N_B = 5$, $\beta = 0.6263$ (3/8 full tank), $\frac{h_o}{a} \cong 0.4999$, $\theta_c = 5.06°$, ($\Gamma = -38.430$, $V_L = 1.35$).† 12×9 mesh (non-uniform on free surface) yielded $\frac{\omega_1^2 a}{g} = 1.114$‡, $\frac{m_1}{\rho V_L} = 0.582$, $z_1 = -0.5841$ compared with Lockheed result of $\frac{\omega_1^2 a}{g} = 0.966$. It is noted that the value of z_1 puts the first mass under the tank bottom which should be examined by future experiments when available.

*Calculated for 3/4-full tank.

†For $\theta_c = 5.06°$, the Γ used in ASME paper APM-EEE was in error and the correct value is given here as are the results.

‡With 23×17 mesh, $\frac{\omega_1^2 a}{a} = 1.079$, $\frac{m_1}{\rho V_L} = 0.5736$, $z_1 = -0.4644$; and $\frac{\omega_2^2 a}{g} = 15.03$ while Lockheed's result for $\frac{\omega_2^2 a}{g}$ is 13.26. It is uncertain which results are more accurate. The value of Γ has not been given by Lockheed to facilitate the explanation of the differences.